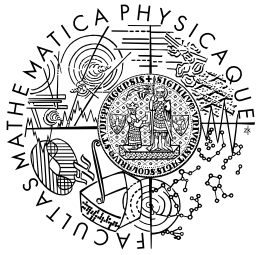

FACULTY
OF MATHEMATICS
AND PHYSICS
Charles University

MASTER THESIS

Jakub Dolejší

Dynamical signatures of quantum phase transitions for excited states

Institute of Particle and Nuclear Physics

Supervisor of the bachelor thesis:	prof. RNDr. Pavel Cejnar, Dr., DSc.
Study programme:	Physics
Study branch:	Nuclear and Subnuclear Physics

Prague 2020

I declare that I carried out this master thesis independently, and only with the cited sources, literature and other professional sources. It has not been used to obtain another or the same degree.

I understand that my work relates to the rights and obligations under the Act No. 121/2000 Sb., the Copyright Act, as amended, in particular the fact that the Charles University has the right to conclude a license agreement on the use of this work as a school work pursuant to Section 60 subsection 1 of the Copyright Act.

In Divec, July 20, 2020 Jakub Dolejší

To everybody with whom I shared all the wonderful experiences.
A special thanks to those who stayed during hard times.

Title: Dynamical signatures of quantum phase transitions for excited states

Author: Jakub Dolejší

Institute: Institute of Particle and Nuclear Physics

Supervisor: prof. RNDr. Pavel Cejnar, Dr., DSc., Institute of Particle and Nuclear Physics

Abstract: We study the impact of quantum phase transitions (QPTs) and excited-state quantum phase transitions (ESQPTs) on the validity of the adiabatic approximation for a slowly varying Hamiltonian. We compare two cases, when the initial state is the ground state of the initial Hamiltonian and when the initial state is a statistical mixture of excited states induced by a finite temperature. We use the Lipkin-Meshkov-Glick model of a spin lattice and obtain an abruptly decreasing scaling law of the ground-state population with a growing system size N. We comment on the justifiability of using the Landau-Zener formula to make a quantitative prediction in the case of a first-order and a second-order QPT.

To achieve a truly adiabatic evolution in the thermodynamic limit, one would need to perform the Hamiltonian change during an impossibly long time period. It is possible, however, to obtain the same adiabatic final state in a given finite time period by inducing the quantum evolution with another Hamiltonian specifically devised for this purpose, thus employing the so called adiabatic shortcut. We verify the validity of adiabatic shortcuts in the presence of QPTs and ESQPTs and study the costs of performing such adiabatic shortcuts.

Keywords: Quantum phase transitions, Excited-state quantum phase transitions, Adiabatic approximation, Adiabatic shortcuts, Counter-diabatic driving, Lipkin-Meshkov-Glick model

Contents

Introduction **3**

1 Quantum phase transitions **5**
1.1 Ground-state quantum phase transitions . . . 5
1.2 Excited-state quantum phase transitions . . . 5
1.3 Quantum simulation of quantum phase transitions . . . 6

2 Transitionless external driving **8**
2.1 Adiabatic approximation . . . 8
2.2 Landau-Zener transitions . . . 8
2.3 Adiabatic shortcuts . . . 10
2.4 Adiabatic shortcut costs . . . 11
2.5 Thermal state . . . 13
2.6 Fidelity . . . 13

3 Lipkin-Meshkov-Glick model **15**
3.1 Spin formulation . . . 15
3.2 Classical correspondence . . . 16
3.3 Quantum phase transition . . . 17
3.4 Excited-state quantum phase transition . . . 17
3.5 Minimum energy gap . . . 19

4 Adiabatic and non-adiabatic driving **20**
4.1 System dynamics . . . 20
4.2 Scaling of the ground-state population . . . 21
4.2.1 Applicability of the Landau-Zener formula . . . 21
4.2.2 Two-level approximation . . . 23
4.2.3 Landau-Zener region . . . 23
4.2.4 Scaling with system size . . . 26
4.2.5 Adiabatic driving rate . . . 28
4.3 Non-zero temperature . . . 28
4.3.1 Thermal state dynamics . . . 29
4.3.2 Optimum temperature . . . 32

5 Counter-diabatic driving **35**
5.1 System dynamics . . . 35
5.2 Shortcut cost . . . 35

Conclusion **37**

A No-crossing theorem **39**

B Geometric phase **40**
B.1 Imaginary exponent . . . 40
B.2 Time independence . . . 40

C More on Fidelity **42**

Bibliography **44**

Introduction

The development of quantum computers and related methods of manipulation with matter on the quantum level has been, among other, opening a direct experimental access to real-time quantum dynamics [1–3] during the last decades. The principle behind quantum computers is to store binary information as a state of a two-level quantum system, a *quantum bit (qubit)*. To carry out a computation, one applies a series of quantum gates (e.g. logical and arithmetic gates) which change the state of a certain subset of qubits. In this manner, one ultimately devises algorithms to run on a quantum computer [4]. In the end, one has to decode the result of the computation from a repeated execution of such a quantum program because of the probabilistic nature of a quantum measurement. In this sense, quantum computers represent a quantum equivalent of classical computers which are also based on a systematic application of logical and arithmetic gates. The size of quantum computers has already reached several tens of qubits and it keeps increasing [5–7].

There is another similar concept of using quantum properties of matter to perform computations, the so called *adiabatic quantum computers* or *quantum annealers* [8, 9]. Their sizes are currently reaching a few thousands of qubits [10–12] (however the size of a quantum computer and that of an adiabatic quantum computer are incomparable quantities). The principle lies in encoding a problem into a Hamiltonian whose ground state represents the solution to the corresponding problem (and one a priori does not know the form of such a ground state). The method to bring the adiabatic quantum computer into the desired ground state exploits the adiabatic theorem [13, 14]. It has to be possible to set the physical system of an adiabatic quantum computer into a ground state of a given conventional Hamiltonian (the default setting of the computer). Then one very slowly varies the parameters of this system so that its Hamiltonian continually changes from the initial conventional one to the final desired one. As one modifies the Hamiltonian slowly, the system remains in its instantaneous ground state. Consequently, we arrive at the desired ground state which we simply measure and thus obtain the solution to our problem.

One significant detail was left unmentioned and that is how slowly we have to vary the Hamiltonian in order to avoid system excitations and to obtain the correct solution. The speed is determined by the energy gap between the ground state and the first excited state, or more generally on the energy spacing in the vicinity of the current state of the adiabatic quantum computer [15–17]. A serious problem of inconceivably large time periods arises in the presence of QPTs [18, 19] and ESQPTs (see section 4.2.5) which represent non-analyticities respectively in the ground state and in the excited-state spectrum with varying Hamiltonian parameters. QPTs and ESQPTs are related with extreme eigenstate approaching. The energy spacing even goes to zero in the true thermodynamic limit (infinite system size $N \to \infty$). We will demonstrate that such critical phenomena can take place even in a very simple U(2)-based Lipkin-Meshkov-Glick (LMG) model [20] and we will study the divergence rate for a Hamiltonian with an ESQPT accompanying a QPT of a first order and of a second order.

Fortunately, there exists another method of driving the system with a specif-

ically devised Hamiltonian which induces such an evolution during which the system remains in exact instantaneous eigenstates of the true Hamiltonian of interest. This procedure is called an *adiabatic shortcut* or a *counter-diabatic driving* and it enables to perform the same transition between Hamiltonians in an arbitrary time period [21, 22]. In order to be able to perform an adiabatic shortcut, one has to know the form of instantaneous eigenstates throughout the evolution – which is tractable in a good deal of models. The concept of adiabatic shortcuts was already experimentally verified [23] and a quantum shortcut through a QPT was theoretically covered [24]. We will demonstrate the applicability of adiabatic shortcuts in the presence of an ESQPT and we will study the complexity or costs of their execution.

1. Quantum phase transitions

1.1 Ground-state quantum phase transitions

Suppose a Hamiltonian which depends continuously on a real *control parameter* λ (e.g. an internal coupling constant or an external field strength). Traditionally, a *quantum phase transition (QPT)* is understood as a non-analyticity in the ground-state energy as a function of non-thermal parameter λ. In other words, one of the (higher) derivatives with respect to λ exhibits a discontinuity or a divergence at a critical value λ_c. It has to be noted that a system can manifest a true non-analyticity only in the thermodynamic limit. However, finite-sized systems exhibit already certain precursors of a critical behaviour.

One can apply the Ehrenfest classification to QPTs after restricting oneself on the cases with a jump discontinuity in one of the derivatives. If the first derivative manifests a jump discontinuity, the QPT is said to be of the first order. The corresponding function is continuous but non-smooth at λ_c. In a general *n-th order QPT* the first $n-1$ derivatives are continuous and the n-th one exhibits a jump discontinuity.

To describe in which quantum phase the system is found, one makes use of a well-chosen observable called the *order parameter*. It is such a quantity whose value is identically zero in one of the phases and non-zero in the other. A jump discontinuity (a divergence) in the n-th derivative of the ground-state energy is equivalent to a jump discontinuity (a divergence) in the $(n-1)$th derivative of the order parameter.

Based on the behaviour of the order parameter at the critical point λ_c, one can define a more general classification of QPTs. A *continuous QPT* corresponds to a continuous order parameter with a discontinuity or a divergence in one of its higher derivatives. On the contrary, for a *discontinuous QPT*, the discontinuity or the divergence is present already in the order parameter itself. The first-order QPT is categorized as a discontinuous transition whereas all the higher-order QPTs are continuous transitions.

1.2 Excited-state quantum phase transitions

An *excited-state quantum phase transition (ESQPT)* represents a generalization of the concept of a QPT to excited states, thus, an ESQPT is a non-analyticity in the whole spectral plane $E \times \lambda$. However, this non-analyticity doesn't have to show up in the individual excited states. It manifests as a non-analytic change of spectral properties such as the level density, level flow or expectation values of some observables. There exists an extensive literature on ESQPTs, see e.g. [25–33] for general studies and [34–40] for ESQPTs in the LMG model. This phenomenon defines a critical ESQPT energy which can depend non-trivially on λ.

Non-analyticities in the quantum spectrum are tightly connected with stationary points of the classical Hamiltonian. This correspondence as well as ESQPT classification is studied in detail in [32]. In particular, a non-analyticity in the global minimum of the classical Hamiltonian translates as a ground-state QPT,

whereas all the other non-analyticities belong to ESQPTs. ESQPTs corresponding to degenerate stationary points are not classifiable. On the other hand, ESQPTs corresponding to non-degenerate stationary points can be classified based on two parameters: the number of degrees of freedom f of the system and the index r of the stationary point (the number of Hessian negative eigenvalues).

The irregular part of the smoothed level density $\bar{\rho}$ in the vicinity of the critical energy E_c reads [32]

$$\frac{\partial^{f-1}\bar{\rho}}{\partial E^{f-1}} \propto \begin{cases} (-1)^{\frac{r+1}{2}} \log|E - E_\mathrm{c}| & \text{for } r \text{ odd}\,, \\ (-1)^{\frac{r}{2}} \quad \theta(E - E_\mathrm{c}) & \text{for } r \text{ even}\,, \end{cases} \tag{1.1}$$

where θ is the Heaviside step function. The $(f-1)$th derivative of $\bar{\rho}$ manifests either a logarithmic divergence or a jump discontinuity. A significant result is that the effect of ESQPTs decreases with a growing number of degrees of freedom. In order to observe an ESQPT, the system has to manifest a sort of a collective behaviour (a low number of degrees of freedom). Remember that at the same time, one needs a large system (the thermodynamic limit) to obtain the non-analyticity itself.

We will encounter ESQPTs of type $(f, r) = (1, 1)$ and $(f, r) = (1, 0)$, i.e. a local maximum and a local minimum of a two-dimensional Hamiltonian ($\dim = 2f$). The maximum manifests as a logarithmic divergence of the state density and the minimum as a jump discontinuity. As we have to treat numerically a finite-sized system, the precursor of the ESQPT of type $(1, 1)$ will be shown as a sharp increase in the energy level density. In spite of this high density, no two states will become degenerate at any point thanks to the no-crossing theorem (appendix A). Therefore, the ordering of the energy states is unambiguously conserved and each pair of neighbouring states which approach each other will stop doing so at a certain point and start separating again, thus creating a so called *avoided crossing* or an *anti-crossing*.

1.3 Quantum simulation of quantum phase transitions

The value of some types of control parameters (e.g. external field strengths) is easily changed. Such control parameters can be used to drive a quantum system. In contrast, other types of control parameters (e.g. coupling constants, hopping parameters) typically have a fixed value in nature. To give an example, hopping parameters in the Hubbard model [3] are given by the lattice spacing and by the characteristics of the particles in the lattice. Consequently, they do not allow continuous external driving. What is possible to study are the characteristics of a system under different values of such control parameters. This allows one to understand how can essentially the same microscopic system lead to totally different dynamical characteristics of a macroscopic body. For instance, there is a QPT between a conducting phase and an insulating phase in the case of the Hubbard model.

The variation of an external field is sometimes equivalent to a variation of an internal coupling constant as the Hamiltonian (up to the overall scale) depends

only on the ratio of these terms. Apart from this, it might seem as if studying a dynamical response of a system which is being driven through a QPT was a purely theoretical endeavour. However, there is a way to experimentally access this phenomenon with the use of quantum simulators.

Quantum simulation [41] is a process in which one quantum system is used to emulate the behaviour of another quantum system based on a mathematical mapping between these systems. In practice, one uses a well-controlled system to obtain results for a system which can be otherwise experimentally inaccessible. For example, quantum simulations of QPTs in the Ising model were realized using ultracold atoms [42] or trapped ions [43, 44].

Physical implementations of quantum simulators are artificially created in a way that their parameters can be tuned. In the case of ultracold atoms in an optical lattice, the lattice spacing depends on the laser wavelength and the depth of the trapping potential depends on the laser intensity [45]. Hence, a naturally fixed parameter can be cast onto a modifiable one in a suitable quantum simulator. In summary, it makes good sense to study external driving of all sorts even for naturally inaccessible control parameters.

2. Transitionless external driving

2.1 Adiabatic approximation

Suppose a Hamiltonian $\hat{H}_0(t)$ which depends explicitly on time t. Let $|n(t)\rangle$ be the n-th instantaneous eigenstate of $\hat{H}_0(t)$, which satisfies

$$\hat{H}_0(t)\,|n(t)\rangle = E_n(t)\,|n(t)\rangle\ . \tag{2.1}$$

Remember that the solution of the time-dependent Schrödinger equation in general is not equal to the instantaneous eigenstates. We suppose that the energy eigenstates do not cross each other (appendix A), hence there are no ambiguities in the state numbering throughout the whole spectrum $E \times \lambda$.

The concept of adiabatic evolution comes from the setting in which the characteristic timescale τ_{T} of the Hamiltonian change (T for transition) is far greater than the characteristic timescale τ_{H} of the quantum evolution of the system (sometimes called the Heisenberg time). Now, we only need to consider that τ_{H} changes along with the changing Hamiltonian and that also the rate of the external driving might vary in time,

$$\tau_{\mathrm{T}}(t) \gg \tau_{\mathrm{H}}(t) \qquad \forall t\,. \tag{2.2}$$

A representative value $\tau_{\mathrm{H}}(t)$ for a multi-level Hamiltonian can be obtained from the smallest energy difference $\Delta E(t)$ between any state occupied at time t and one of its neighbouring states,

$$\tau_{\mathrm{H}}(t) = \frac{1}{\Delta E(t)}\,. \tag{2.3}$$

Note that in literature the Heisenberg time is usually defined using the mean spacing of nearest neighbours [46] instead of using simply the closest occupied pair of states.

The adiabatic theorem [13, 14] states that if the system starts in its n-th eigenstate at time $t = 0$,

$$|\psi_n(t=0)\rangle = |n(t=0)\rangle\ , \tag{2.4}$$

then it will remain in the corresponding instantaneous eigenstate up to an additional geometric phase factor (and the usual dynamical phase factor),

$$|\psi_n(t)\rangle = \exp\left(-i\int_0^t \mathrm{d}t' E_n(t')\right) \exp\left(-\int_0^t \mathrm{d}t' \left\langle n(t')\middle|\frac{\partial}{\partial t'}\middle|n(t')\right\rangle\right) |n(t)\rangle\ , \tag{2.5}$$

where we hold $\hbar = 1$. As shown in appendix B, $\langle n(t')|\frac{\partial}{\partial t'}|n(t')\rangle$ is purely imaginary and therefore the second term truly is an additional phase factor.

2.2 Landau-Zener transitions

It is only within the adiabatic approximation that the system remains in the instantaneous eigenstate. If the Hamiltonian change happens in a finite time

period, the remaining eigenstates will also get populated during the evolution (a multi-level analogue of Landau-Zener transitions).

The classical Landau-Zener (LZ) problem [15–17] is that of an evolution of a ground state in a class of time-dependent Hamiltonians represented by

$$\hat{H}_{\mathrm{LZ}}(t) = \begin{pmatrix} \frac{\gamma t}{2} & \beta \\ \beta^* & -\frac{\gamma t}{2} \end{pmatrix} , \tag{2.6}$$

where $\gamma > 0$ and $\beta \in \mathbb{C}$. The time-dependent eigenvalues are plotted in fig. 2.1. Parameter γ represents the rate of growth of the energy difference between the ground state and the excited state as $t \to +\infty$. On the other hand, the minimum value of the energy gap between the two eigenstates reads $\Delta E = 2|\beta|$ and it takes place at $t = 0$.

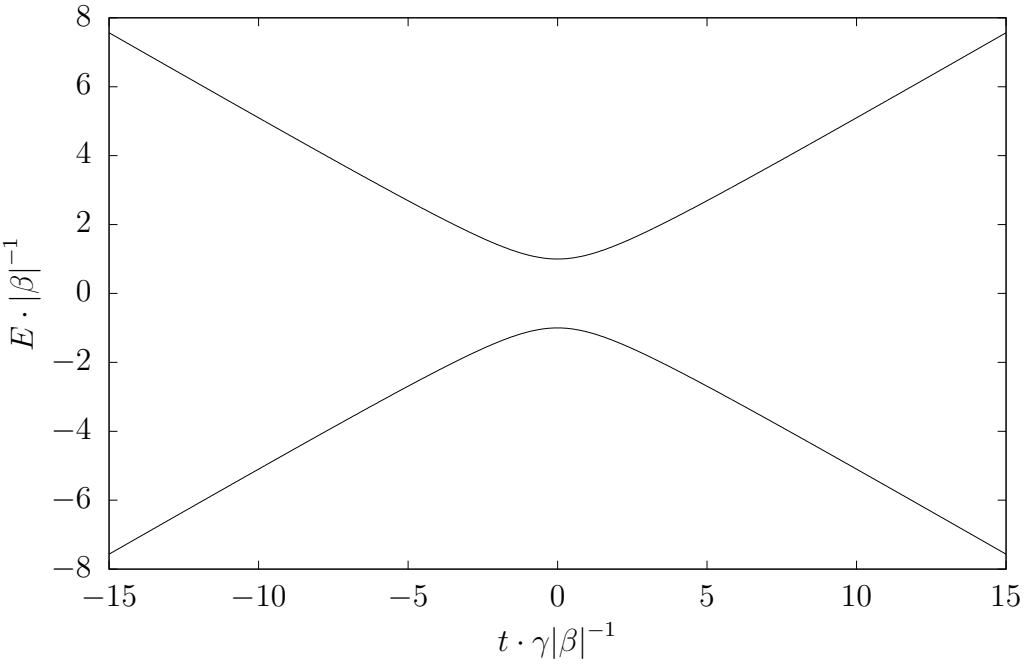

Figure 2.1: The avoided crossing in the spectrum of $\hat{H}_{\mathrm{LZ}}(t)$

One starts with a system in the ground state at $t = -\infty$ and is interested in the population of the excited state at $t = +\infty$. This probability reads

$$P_{\mathrm{exc}} = \exp\left(-2\pi \frac{\Delta E^2}{4\gamma}\right) . \tag{2.7}$$

The expression holds generally for any two-level avoided crossing, i.e. the eigenenergy asymptotes can have arbitrary directions. In this general case, γ is given by

$$E_1^{\infty}(t) - E_0^{\infty}(t) = \gamma t \, , \tag{2.8}$$

where $E_0^{\infty}(t)$ and $E_1^{\infty}(t)$ represent the asymptotes of the ground state and of the excited state.

In our case, the driving of the Hamiltonian $\hat{H}(\lambda)$ will be carried out by a time-dependent control parameter $\lambda(t)$. Let λ be varied from λ_{i} to $\lambda_{\mathrm{f}} = \lambda_{\mathrm{i}} + \Delta\lambda$ with

a constant rate $\dot{\lambda}$ over time period $\tau = \Delta\lambda/\dot{\lambda}$. In this case, it is more practical to define a purely geometrical analogue of γ,

$$\alpha = \frac{\tau}{\Delta\lambda}\gamma = \frac{\gamma}{\dot{\lambda}}\,, \tag{2.9}$$

for which it holds

$$E_1^\infty(\lambda) - E_0^\infty(\lambda) = \alpha\lambda\,. \tag{2.10}$$

The LZ excitation probability now reads

$$P_{\text{exc}} = \exp\left(-2\pi\frac{\Delta E^2}{4\alpha\dot{\lambda}}\right)\,. \tag{2.11}$$

As already stated before, probability P_{exc} becomes negligible in the adiabatic approximation $\dot{\lambda} \to 0$ ($\tau \to \infty$). However, now we see that LZ transitions might occur even for slow Hamitonian changes if the energy distance of eigenstates gets very close to zero during the evolution. This phenomenon happens in the presence of QPTs as they imply avoided crossings of energy levels (or even real crossings, for which $\Delta E = 0$).

2.3 Adiabatic shortcuts

It is possible to devise a Hamiltonian $\hat{H}(t)$ closely related to $\hat{H}_0(t)$ so that it induces evolution which follows the instantaneous eigenstates of $\hat{H}_0(t)$. In other words, we want to reconstruct a Hamiltonian $\hat{H}(t)$ for which it holds

$$i\frac{\partial}{\partial t}\left|\psi_n(t)\right\rangle = \hat{H}(t)\left|\psi_n(t)\right\rangle \quad \forall n\,, \tag{2.12}$$

where the instantaneous eigenstates $|\psi_n(t)\rangle$ are defined by the adiabatic theorem (2.5), i.e. we choose to keep the geometric phase. Berry [21] derives that such a Hamiltonian is given by the following formula,

$$\hat{H}(t) = \hat{H}_0(t) + i\sum_{m\neq n}\sum_n \frac{\left\langle m(t)\right|\frac{\partial}{\partial t}\hat{H}_0(t)\left|n(t)\right\rangle}{E_n(t) - E_m(t)}\left|m(t)\right\rangle\!\left\langle n(t)\right|\,, \tag{2.13}$$

where $E_n(t)$ is the n-th instantaneous eigenvalue of $\hat{H}_0(t)$ as given by (2.1). Remark also that the additional term is strictly off-diagonal in the instantaneous eigenbasis.

Let us now suppose that the Hamiltonian is of the following form,

$$\hat{H}_0(t) = \hat{\mathcal{T}} + \lambda(t)\hat{\mathcal{V}}\,. \tag{2.14}$$

It is possible to reexpress the correction $\hat{H}'(t) = \hat{H}(t) - \hat{H}_0(t)$ as

$$\left\langle m(t)\right|\hat{H}'(t)\left|n(t)\right\rangle = i\frac{\partial\lambda(t)}{\partial t}\,\frac{\left\langle m(t)\right|\hat{\mathcal{V}}\left|n(t)\right\rangle}{E_n(t) - E_m(t)}\left(1 - \delta_{mn}\right). \tag{2.15}$$

Let us call the time derivative $\dot{\lambda}(t)$ the *driving rate* as it represents the speed of the external driving.

Suppose that in terms of matrix elements all three operators $\hat{H}_0(t)$, $\hat{\mathcal{T}}$ and $\hat{\mathcal{V}}$ are comparable in magnitude. Then the last expression clearly states that as a necessary condition for the adiabatic approximation to hold we need to vary the control parameter λ very slowly, that being

$$\dot{\lambda}(t) \ll \Delta E(t)\,, \tag{2.16}$$

where $\Delta E(t)$ is the smallest instantaneous-energy difference between any two states at time t (let us now discard the possibility that the energetically closest states might not be occupied at all). An easy way to satisfy the adiabaticity condition is to set a constant driving rate for which it holds

$$\dot{\lambda} \ll \Delta E = \min_t \Delta E(t)\,. \tag{2.17}$$

In order to accelerate the whole process, it would also be possible to continually readjust the driving rate according to $\Delta E(t)$.

Note however, that even with (2.17) satisfied, the small corrections (2.15) can add up during the integration of the Schrödinger equation into adiabaticity violation. As we will prove the LZ aproximation (2.11) to a certain extent, we can already reveal that a stronger condition,

$$\dot{\lambda} \ll \frac{\Delta E^2}{\alpha}\,, \tag{2.18}$$

will have to hold.

2.4 Adiabatic shortcut costs

The employment of an adiabatic shortcut involves creating a new physical phenomenon – which requires energy. For example, for a spin driven by a magnetic field, the adiabatic shortcut is implemented by yet another time-dependent magnetic field [21]. The energy of the spin itself can even decrease after turning the shortcut field on. On the other hand, the creation of the new magnetic field can be quite costly in terms of energy.

However, Hamiltonian $\hat{H}_0$ (and thus also $\hat{H}'$) typically describes only the state of the system (qubits), not of the magnetic field surrounding it. That is why interpreting expressions like $\langle\psi|H'|\psi\rangle$ as the energy cost of an adiabatic shortcut does not work. Moreover, in this particular case, one obtains $\langle\psi|H'|\psi\rangle = 0$ because $\hat{H}'$ was constructed as strictly off-diagonal in the basis of instantaneous eigenstates (and the system stays in the instantaneous ground state during the counter-diabatic evolution). Further, the expression for such an energy cost has to vary accordingly with the physical phenomenon implementing the adiabatic shortcut (different for each system).

There is, however, another general way to quantify the complexity of an adiabatic shortcut. Let us first focus on the properties that one might expect from such a quantity. If direct driving with $\hat{H}_0$ results in a practically adiabatic passage, the costs of the corresponding shortcut should be close to zero. On the other hand, the closer two eigenstates are, the stronger they interact. Therefore, preventing transitions in the neighbourhood of a QPT should be very difficult. To

summarize, we will try to find a function of the Hamiltonian which has some sort of a characteristic behaviour (e.g. an enhanced growth rate or even a distinctive peak) at each avoided crossing through which the system is driven.

The form of Hamiltonian $\hat{H}'(t)$ was derived so that it suppresses all transitions induced by $\hat{H}_0(t)$. Therefore, the moduli of matrix elements of $\hat{H}'$ represent exactly the strength of interaction between pairs of individual instantaneous eigenstates in the case when the system is driven directly by $\hat{H}_0$. Without any further insight, one might try computing the Frobenius norm of $\hat{H}'(t)$,

$$\left\|\hat{H}'\right\|_{\mathrm{F}} = \sqrt{\mathrm{Tr}\left[\hat{H}'\hat{H}'^{\dagger}\right]} = \sqrt{\sum_{mn}\left|\left\langle m\middle|\hat{H}'\middle|n\right\rangle\right|^2}\,, \tag{2.19}$$

only to quickly find out that it incorporates a peak at each avoided crossing in the entire excited spectrum of $\hat{H}_0$.

The remedy is to include only those elements of $\hat{H}'$ which correspond to the transition of the current state $|\psi(t)\rangle$ of the system into all possible states,

$$\mathcal{M} = \sqrt{\sum_{m}\left|\left\langle m\middle|\hat{H}'\middle|\psi\right\rangle\right|^2} = \sqrt{\left\langle\psi\middle|\hat{H}'^2\middle|\psi\right\rangle}\,. \tag{2.20}$$

We denoted this quantity $\mathcal{M}$ for it corresponds to an effective matrix element for transitions of the current system state. In the relevant case for adiabtic quantum computing, we simply let $|\psi(t)\rangle = |0(t)\rangle$. Since $\hat{H}'$ is off-diagonal, $\mathcal{M}$ now has a zero contribution from the "transition" from the ground state $|\psi\rangle = |0\rangle$ to the ground-state $|m\rangle = |0\rangle$. Therefore $\mathcal{M}(t)$ represents the strength of adiabaticity-violating transitions as a function of time.

It is possible to summarize function $\mathcal{M}(t)$ with a single number as well as to reacquire physical insight into the cost of adiabatic shortcuts with the use of the Fermi golden rule,

$$\Gamma_{i\to f} = 2\pi\left|\,\langle f|\hat{H}'|i\rangle\right|^2\rho(E_f)\,. \tag{2.21}$$

The rule states that the transition rate $\Gamma_{i\to f}$ from state $|i\rangle$ to state $|f\rangle$ is proportional to the squared matrix element of the interaction Hamiltonian and to the density of states at the energy of state $|f\rangle$. Therefore, we can define cost $\mathcal{C}$ of an adiabatic shortcut by integrating the Fermi rule over all possible (discrete) final states and over the whole evolution time,

$$\begin{aligned}\mathcal{C} &= 2\pi\int_0^\tau\sum_m\left|\left\langle m(t)\middle|\hat{H}'(t)\middle|\psi(t)\right\rangle\right|^2\mathrm{d}t = \\ &= 2\pi\int_0^\tau\mathcal{M}^2(t)\mathrm{d}t = \frac{2\pi}{\dot{\lambda}}\int_{\lambda_\mathrm{i}}^{\lambda_\mathrm{f}}\mathcal{M}^2(\lambda)\mathrm{d}\lambda\,,\end{aligned} \tag{2.22}$$

and obtain the total volume of inhibited transitions. Since this cost originates from the Fermi rule, its dimension is energy (there is a missing $\hbar = 1$ term in the denominator). Coming back to (2.15), we see that the transition matrix element is proportional to the driving rate, $\mathcal{M} \propto \dot{\lambda}$. Hence also the adiabatic shortcut cost is proportional to the driving rate, $\mathcal{C} \propto \dot{\lambda}$.

We could have as well obtained another plausible definition of an adiabatic shortcut cost by taking simply the maximum of $\mathcal{M}(\lambda)$. The results for either cost would be probably qualitatively quite similar because $\mathcal{M}$ has a peak at the QPT which accounts for the most part of the integral in (2.22). Some physical insight into this shortcut cost stems froms noticing that $\mathcal{M}^2(\lambda)$ is in fact the energy variance of $|\psi\rangle$ defined by the additional Hamiltonian term $\hat{H}'$.

2.5 Thermal state

An ESQPT is by its nature a phenomenon affecting excited states. The energy level spacing ΔE (restricted to occupied states and their neighbours) differs for evolutions driven through distinct eigenstates. Therefore, one could investigate how the dynamical impact of an ESQPT changes when the system enters the critical region from states with different energies. In this respect, we will only compare the end-state in the case where the systems starts from the ground state (zero temperature) and where it starts from the *thermal state* corresponding to a finite temperature T. The thermal state represents a canonical ensemble (i.e. a statistical mixture) of individual excited eigenstates. It can be described by a density matrix using the Maxwell-Boltzmann distribution [47, 48] as

$$\hat{\rho}_T(\hat{H}_0) = \frac{1}{Z(T)} \exp\left(-\frac{\hat{H}_0}{kT}\right), \tag{2.23}$$

$$Z(T) = \mathrm{Tr}\left[\exp\left(-\frac{\hat{H}_0}{kT}\right)\right] = \sum_n \exp\left(-\frac{E_n}{kT}\right), \tag{2.24}$$

where $Z(T)$ is the partition function and E_n are the eigenenergies of $\hat{H}_0$. For computational purposes, we let the Boltzmann constant $k = 1$.

The *thermalization* of a system is a process of acquiring equilibrium with a thermal reservoir. The process is described by a characteristic timescale. Supposing that the timescale of quantum dynamics is significantly smaller than the thermalization timescale, one can start with a fully thermalized initial state and then simply carry out a purely quantum evolution on each of the states from the original statistical mixture. In terms of the system density matrix $\rho(t)$,

$$\begin{aligned}\hat{\rho}(t=0) &= \hat{\rho}_T\Big(\hat{H}_0(t=0)\Big) = \\ &= \sum_n \frac{1}{Z(T)} \exp\left(-\frac{E_n(0)}{kT}\right) |n(0)\rangle\langle n(0)| \stackrel{\text{def}}{=} \\ &\stackrel{\text{def}}{=} \sum_n p_n |n(0)\rangle\langle n(0)| , \end{aligned} \tag{2.25}$$

$$\hat{\rho}(t) = \sum_n p_n \hat{U} |n(0)\rangle\langle n(0)| \hat{U}^\dagger , \tag{2.26}$$

where $\hat{U}$ is the evolution operator from time 0 to t.

The described procedure represents a quantum evolution of a system in a weak contact with a thermal reservoir (i.e. the thermalization timescale is very long). Alternatively, it can be interpreted as first letting the system equilibrate in contact with a thermal reservoir and only before starting the driven evolution putting them apart and isolating the system again. This interpretation will have to be considered when approaching the adiabtic limit by taking a very small driving parameter $\dot{\lambda}$.

2.6 Fidelity

Since adiabatic quantum computing is based on finding the ground state of a given Hamiltonian, the aim of the external driving procedure is to obtain as high

a ground-state population as possible. Hence, it is possible to quantify the quality of a performed external driving protocol by the *fidelity* [49, 4] of the obtained final state $\hat{\rho}(\tau)$ and the ground state $\hat{\rho}_0(\tau) = |0(\tau)\rangle\langle 0(\tau)|$ of the final Hamiltonian $\hat{H}_0(\tau)$,

$$\mathcal{F}_0(\tau) = \left[\mathrm{Tr} \sqrt{\sqrt{\hat{\rho}_0(\tau)}\hat{\rho}(\tau)\sqrt{\hat{\rho}_0(\tau)}} \right]^2 . \tag{2.27}$$

In the case of a closed quantum system in which we operate only with pure quantum states, the density matrix of the final state $|\psi(\tau)\rangle = \hat{U}\,|\psi(0)\rangle$ is given as $\hat{\rho}(t) = |\psi(\tau)\rangle\langle\psi(\tau)|$ and the fidelity simplifies to a squared inner product of the final state and the desired ground state,

$$\mathcal{F}_0(\tau) = \Big|\, \langle 0(\tau)|\psi(\tau)\rangle \,\Big|^2 . \tag{2.28}$$

If the system is in contact with a thermal reservoir at temperature T, we can use again the simplification that the thermalization timescale is significantly larger than the timescale of system dynamics. Making use of (2.26) one obtains essentially the same result as for a closed quantum system but summed over all the components of the thermal statistical mixture,

$$\mathcal{F}_0(\tau) = \sum_n p_n \Big|\, \Big\langle 0(\tau)\Big|\hat{U}\Big|n(0)\Big\rangle \,\Big|^2 . \tag{2.29}$$

Remark that starting from a pure ground state $|\psi(0)\rangle = |0(0)\rangle$ of the initial Hamiltonian $\hat{H}_0(0)$ corresponds to the thermal state in the zero-temperature limit since for $T = 0$ the weights of the statistical mixture read $p_n = \delta_{n0}$.

To plot the whole evolution of a statistical-mixture state, we will use the fidelity of the current state $\hat{\rho}(t)$ and the k-th instantaneous eigenstate $\hat{\rho}_k(t) = |k(t)\rangle\langle k(t)|$,

$$\mathcal{F}_k(t) = \left[\mathrm{Tr} \sqrt{\sqrt{\hat{\rho}_k(t)}\hat{\rho}(t)\sqrt{\hat{\rho}_k(t)}} \right]^2 . \tag{2.30}$$

Simplifications analogous to (2.28) and (2.29) hold for all values of k. For further details about fidelity see appendix C.

3. Lipkin-Meshkov-Glick model

The Lipkin-Meshkov-Glick (LMG) model was originally created as a simple nuclear model [20]. Its simplicity allows for casting the fermionic operators e.g. onto bosonic operators or spin operators and reinterpreting the model in different contexts. This context always incorporates a multitude of interacting entities which can occur in only two distinct states. We will focus mainly on spin-$\frac{1}{2}$ particles in a lattice.

The newly found virtue of the LMG model lies in our ability to simulate its dynamics both with a classical computer (due to the linear scaling of the Hilbert space dimension with the lattice size N, i.e. the number of spin sites in the lattice) and with quantum simulators (which can be interpreted as a real experimental realization of the system). Its simplicity therefore allows to directly verify first principles of quantum mechanics on a real-time evolution of a quantum system [50, 51].

Since we also want to study ESQPTs, we need to conduct our research on a system with as little degrees of freedom as possible since ESQPT manifestations quickly fade away with the number of degrees of freedom, see equation (1.1). This is yet another reason to choose the LMG model over a more complex one.

3.1 Spin formulation

In the spin formulation, the LMG model describes a simple collective model of spin-$\frac{1}{2}$ lattice placed in a homogeneous magnetic field. The spin-spin interaction doesn't depend on the spin distance at all and thus all the spins interact with each other with the same strength. Therefore, the spin formulation corresponds to the Ising model in the limit of an infinite interaction range.

Thanks to the form of the interaction, it possible to write the Hamiltonian solely in terms of the total spin $\hat{\boldsymbol{J}}$ of the lattice. Terms linear in $\hat{\boldsymbol{J}}$ represent the potential energy of the lattice in a magnetic field and quadratic terms represent the interaction among individual spins. A more detailed analysis can be found in [52, 53].

As a consequence of the form of the Hamiltonian, it holds $\left[\hat{H}, \hat{J}^2\right] = 0$. Thus, the magnitude of the angular momentum j is conserved and we can restrict ourselves on a subspace with fixed j. Let us choose the maximum possible value $j = \frac{N}{2}$. This choice corresponds to a fully symmetrical subspace with respect to an exchange of any pair of spins. The dimension of such a space is dim $= 2j+1 = N+1$ which scales linearly with system size N. Furthermore, the model has only one degree of freedom, the quantum number m (the z-projection of the total angular momentum $\hat{\boldsymbol{J}}$).

We will be using the following two Hamiltonians throughout the thesis,

$$\hat{H}_1(\lambda) = \hat{J}_3 + \lambda\left(-\frac{1}{2j}\left[\hat{J}_1 + c\left(\hat{J}_3 + j\right)\right]^2\right), \tag{3.1}$$

$$\hat{H}_2(\lambda) = \hat{J}_3 + \lambda\left(-\frac{1}{2j}\hat{J}_1^2\right), \tag{3.2}$$

where we set $c = 4$. Hamiltonian $\hat{H}_2$ represents a spin lattice in a transversal magnetic field. Hamiltonian $\hat{H}_1$ has a slightly more complex interaction term (the operator $\hat{J}_3 + j$ represents the number of spins in state $+\frac{1}{2}$). In both cases, control parameter λ represents the spin-spin interaction strength and we will consider only $\lambda > 0$.

Parity conservation in $\hat{H}_2$

Rewriting $\hat{J}_1 = \frac{1}{2}(\hat{J}_+ + \hat{J}_-)$, where $\hat{J}_\pm$ are the usual ladder operators, one sees that all the terms in $\hat{H}_2$ change the quantum number m by 0 or ± 2. Therefore, Hamiltonian $\hat{H}_2(\lambda)$ conserves a parity in the form

$$\hat{\mathcal{P}} = (-1)^{\hat{J}_3 + j} \,. \tag{3.3}$$

Equivalently written $\left[\hat{\mathcal{P}}, \hat{H}_2(\lambda)\right] = 0$, and thus the two operators are simultaneously diagonalizable. Thanks to the no-crossing theorem (appendix A), the eigenstates of $\hat{H}_2(\lambda)$ aren't degenerate and, consequently, they themselves have a good value of parity. Therefore, if the initial state is taken as a state with a good parity (e.g. any instantaneous eigenstate), then only states with the same parity are populated throughout the evolution. In particular, a given instantaneous eigenstate keeps its parity value throughout the adiabatic evolution. For this reason, we will restrict ourselves only on the positive-parity subspace.

3.2 Classical correspondence

It is possible to cast the spin operators in $\hat{H}_{1,2}$ onto position $\hat{x}$ and momentum $\hat{p}$ of a quasiparticle in a potential well by starting from the quasispin ladder operators

$$\hat{J}_\pm = \hat{J}_1 \pm i\hat{J}_2 \,, \tag{3.4}$$

$$\hat{J}_0 = \hat{J}_3 \,, \tag{3.5}$$

using the Holstein-Primakoff mapping [54] onto boson operators and rewriting the boson operators in their standard coordinate-momentum representation,

$$\left(\hat{J}_-, \hat{J}_0, \hat{J}_+\right) \mapsto \left(\sqrt{2j - \hat{b}^\dagger\hat{b}}\;\hat{b},\; \hat{b}^\dagger\hat{b} - j,\; \hat{b}^\dagger\sqrt{2j - \hat{b}^\dagger\hat{b}}\right) , \tag{3.6}$$

$$\left(\hat{b}^\dagger, \hat{b}\right) \mapsto \sqrt{j}\,(\hat{x} - i\hat{p}, \hat{x} + i\hat{p}) \,. \tag{3.7}$$

With this choice of a mapping, the boson operators satisfy the standard commutation relation $\left[\hat{b}, \hat{b}^\dagger\right] = 1$ and the commutation relation of position and momentum reads

$$[\hat{x}, \hat{p}] = \frac{i}{2j} = \frac{i}{N} \,. \tag{3.8}$$

The classical limit, which is usually realized by letting $\hbar \to 0$, is in this case equivalently obtained in the thermodynamic limit $N \to \infty$. And since the true non-analyticities in the Hamiltonian emerge only in the thermodynamic limit, it is possible to employ semiclassical methods to study QPTs and ESQPTs.

The corresponding classical Hamiltonians read

$$\frac{H_1(x,p)}{j} = -1 + (1-\lambda)x^2 + \frac{\lambda}{2}(1-c^2)x^4 - c\lambda x^3\sqrt{2-x^2} + \frac{T_1(x,p)}{j}\,, \tag{3.9}$$

$$\frac{H_2(x,p)}{j} = -1 + (1-\lambda)x^2 + \frac{\lambda}{2}x^4 + \frac{T_2(x,p)}{j}\,, \tag{3.10}$$

where $T_{1,2}(x,p)$ represent generalized kinetic terms.

3.3 Quantum phase transition

The global minimum of a classical Hamiltonian $H(x,p)$ satisfies

$$\frac{\partial H}{\partial x} = 0 \qquad \text{and} \qquad \frac{\partial H}{\partial p} = 0\,. \tag{3.11}$$

Solving this set of equations for $H_1(x,p)$ and $H_2(x,p)$, one obtains for the value of p in both cases $p = 0$ and thus both kinetic terms vanish as $T_{1,2}(x,0) = 0$. Therefore, the search for the ground state reduces to an analysis of the corresponding classical potential.

Potential $V_1(x)$ represents an asymmetric double-well system whose ground-state solution manifests a jump discontinuity in x at $\lambda_{c1} = \frac{1}{1+c^2}$. Potential $V_2(x)$ has the shape of a single well which continuously splits into a parity-symmetric double-well system at $\lambda_{c2} = 1$. The corresponding QPTs are of the first order (discontinuous) for $\hat{H}_1(\lambda)$ and of the second order (continuous) for $\hat{H}_2(\lambda)$.

Irrespective of the exact value of λ within $\lambda < \lambda_c$, the ground state of both Hamiltonians has a fixed value of energy $\frac{E}{j} = -1$. For $\lambda > \lambda_c$ the ground-state energy begins to decrease below this value. Therefore $\hat{H}_1(\lambda)$ and $\hat{H}_2(\lambda)$ describe a transition from a non-interacting phase to an interacting phase with a different type of a QPT.

To return to the spin formulation, in the ground state of the non-interacting phase all the spins are aligned in the direction of the magnetic field (along the negative direction of the z-axis). As we expect this perfect alignment to be broken in the interacting phase, a suitable order parameter is the number of spin-flips in the ground state $\langle \hat{I} \rangle_{\text{gs}}(\lambda) \overset{\text{def}}{=} \langle \hat{J}_3 + j \rangle_{\text{gs}}(\lambda)$ which equals zero in the non-interacting phase.

After crossing a QPT of the first order in $\hat{H}_1$, a sudden change of the magnetization takes place, $\langle \hat{I} \rangle_{\text{gs}}(\lambda_{c1}) \doteq 1.88j$, and as the interaction grows stronger ($\lambda \to \infty$), the system undergoes almost a full inversion $\langle \hat{I} \rangle_{\text{gs}}(\infty) \doteq 1.97j$.

As the QPT in $\hat{H}_2$ is of the second order, the number of spin-flips in this case changes continually from $\langle \hat{I} \rangle_{\text{gs}}(\lambda_{c2}) = 0$ to a state of zero-magnetization $\langle \hat{I} \rangle_{\text{gs}}(\infty) = j$.

3.4 Excited-state quantum phase transition

The ESQPTs correspond to the stationary points in the classical Hamiltonian, i.e. to all of the solutions of (3.11) apart from the ground state and the maximum

energy state. The full solution of this set of equations for both $\hat{H}_1(\lambda)$ and $\hat{H}_2(\lambda)$ is plotted in figs. 3.1 and 3.2 together with all quantum eigenstates to illustrate the changes that happen at ESQPT critical energies.

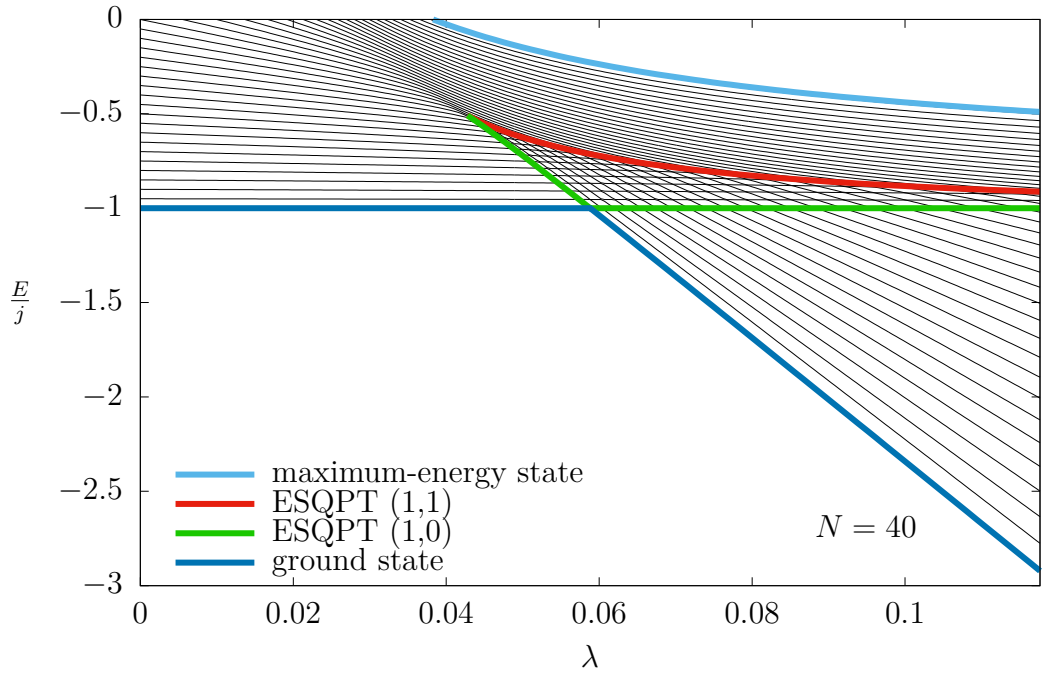

Figure 3.1: The spectrum of $\hat{H}_1(\lambda)$ together with the stationary points of the corresponding classical Hamiltonian.

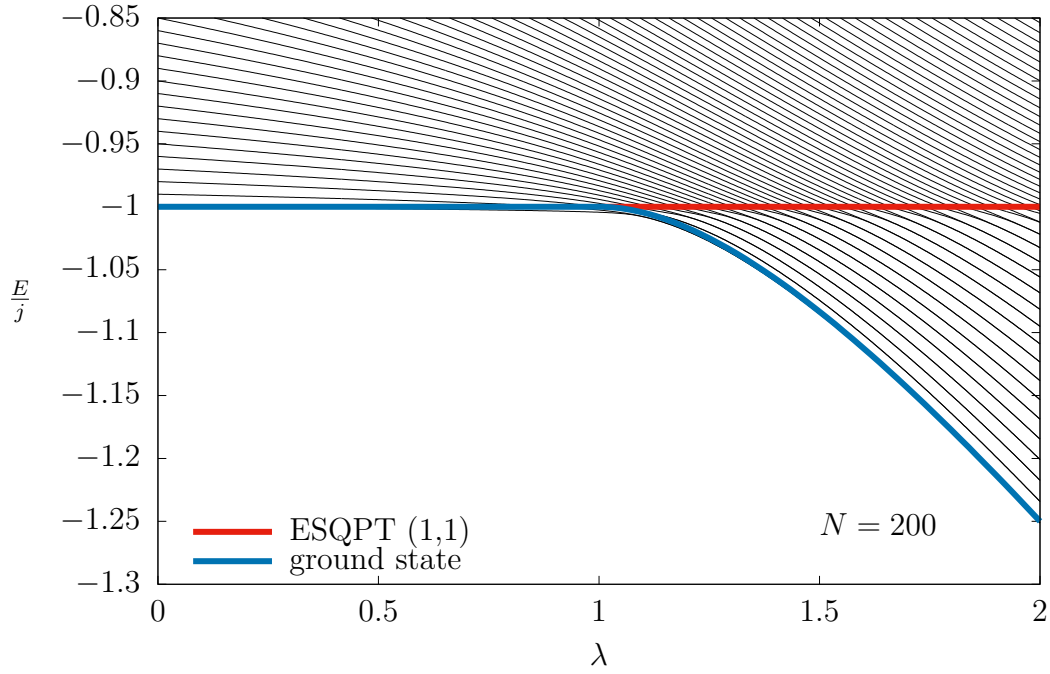

Figure 3.2: The both-parity spectrum of $\hat{H}_2(\lambda)$ together with the stationary points of the corresponding classical Hamiltonian.

The lines representing ESQPTs divide the spectral plane $E \times \lambda$ into distinct regions representing quantum phases. As the stable long-lived state of a system is its ground state, the most important phases are those which contain the ground state in various intervals of the control parameter λ. In the case of $\hat{H}_1$, there is also one phase which concerns only highly excited system states (apart from a small neighbourhood of the QPT). We will not examine this excited phase.

One might be tempted to take the limit $c \to 0$ to obtain fig. 3.2 from fig. 3.1. However, this limit is not graphically very straightforward as there are three QPTs in Hamiltonian $\hat{H}_1(\lambda, c)$ which lie at $c = 2 + \sqrt{2}$, $c = 1$ and $c = 1/\sqrt{3}$.

3.5 Minimum energy gap

Remembering the adiabaticity condition (2.17), the system dynamics qualitatively depends on the smallest energy difference in the Hamiltonian spectrum. Hence it is instructive to have a look at how the minimum energy gap ΔE between the ground state and the first excited state is scaling with the system size N, see fig. 3.3.

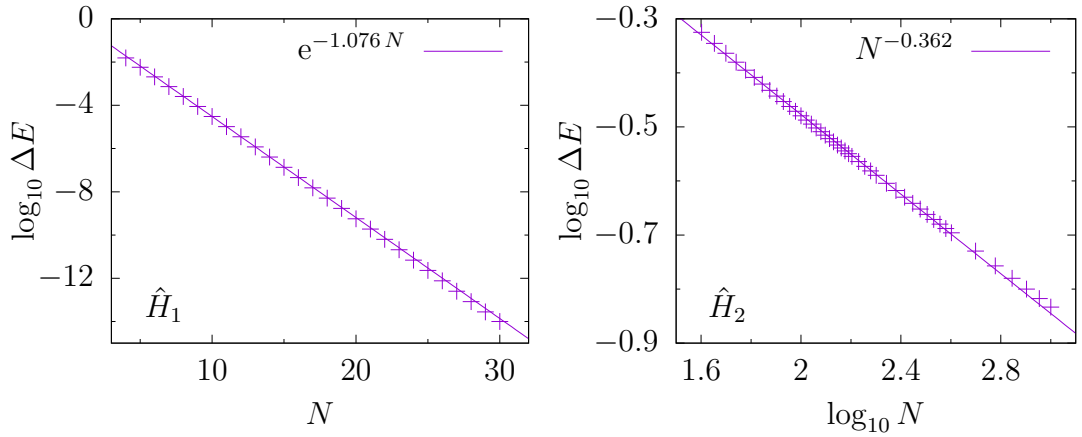

Figure 3.3: Scaling of the minimum energy gap ΔE with system size N for Hamiltonians $\hat{H}_1$ and $\hat{H}_2$. The dependence is fitted by an exponential and a power function, respectively. As we are interested in the scaling for large N, the fit for Hamiltonian $\hat{H}_1$ is done only for $N \geq 10$ (the deviation from the straight line for small N is hidden by the logarithmic scale).

For $\hat{H}_1$ with a discontinuous QPT, the minimum energy gap ΔE decreases approximately exponentially with a growing system size (and one quickly reaches the numerical precision threshold $\sim 10^{-18}$). On the other hand, in the case of a continuous QPT in $\hat{H}_2$, the decrease of ΔE is only algebraic in system size. And in fact, all of the avoided crossings in the spectrum of $\hat{H}_1$ are significantly tighter than those in the spectrum of $\hat{H}_2$.

Therefore to achieve the same level of adiabaticity, one needs to drive much slower a system exhibiting a discontinuous QPT than that exhibiting a discontinuous QPT.

4. Adiabatic and non-adiabatic driving

Both Hamiltonians $\hat{H}_1$ and $\hat{H}_2$ describe a transition from a non-interacting phase to an interacting one, therefore we will seek to compare their behaviour. With this in mind, we will use the common point of zero interaction as the initial point, i.e. $\lambda_\mathrm{i} = 0$. Then, we will evolve the quantum system with a fixed driving rate $\dot{\lambda}$ across the ESQPT up to $\lambda_\mathrm{f} = 2\lambda_\mathrm{c}$. To define the final point in a rather general manner, we used the critical ESQPT point of the corresponding Hamiltonian.

We will first study a direct slow change of the control parameter. As this procedure is in practice simpler than having to employ adiabatic shortcuts, it is of interest to study whether it allows to achieve sufficiently good results (high final population of the ground state) and what are its limits.

4.1 System dynamics

Let us demonstrate the exponential dependence of $\hat{H}_1$ dynamics on system size N and the corresponding fast loss of adiabaticity, see fig. 4.1. Note that the almost adiabatic passage for $N = 4$ is achieved at $\dot{\lambda} = 10^{-6} \approx \Delta E/15500 \approx \Delta E^2/240$.

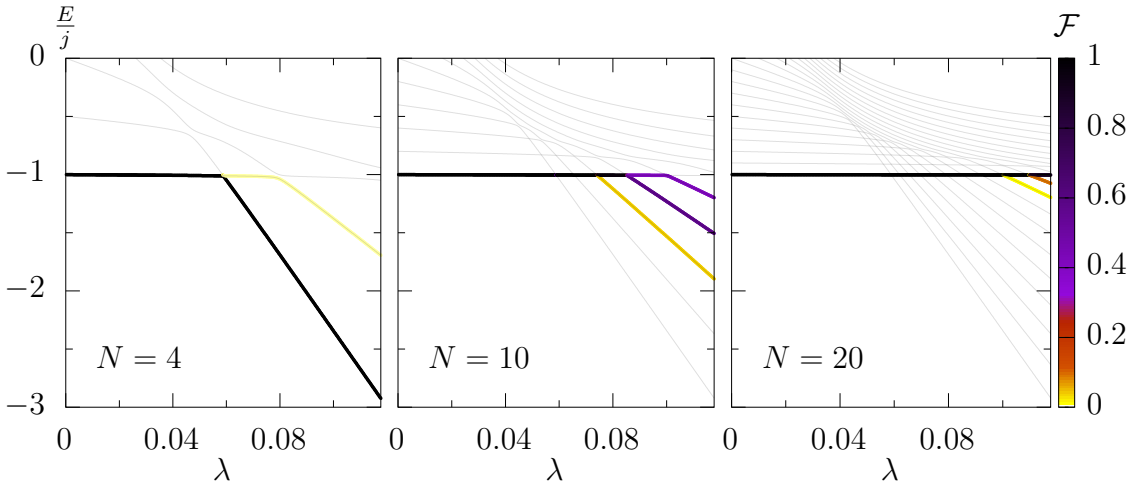

Figure 4.1: Instantaneous eigenstate fidelity $\mathcal{F}_k(t)$ as a function of time during an evolution induced directly by Hamiltonian $\hat{H}_1(\lambda)$ for various system sizes driven at rate $\dot{\lambda} = 10^{-6}$. The system starts in the ground state at $\lambda_\mathrm{i} = 0$.

For numerical reasons, we demonstrate quantum evolution for various values of the driving rate $\dot{\lambda}$ for Hamiltonian $\hat{H}_2$ at $N = 100$. Figure 4.2 shows that for fast driving ($\dot{\lambda} = 2$), the system remains centred at the initial ground-state energy until λ_f. As an effect of a decreasing driving rate, lower excited states get populated. And finally, one obtains an adiabatic passage at $\dot{\lambda} = 0.002$. Notice again that roughly $\dot{\lambda} = 0.002 \approx \Delta E/165 \approx \Delta E^2/55$. We already see an indication that (2.18) is a more suitable condition on adiabaticity than (2.17).

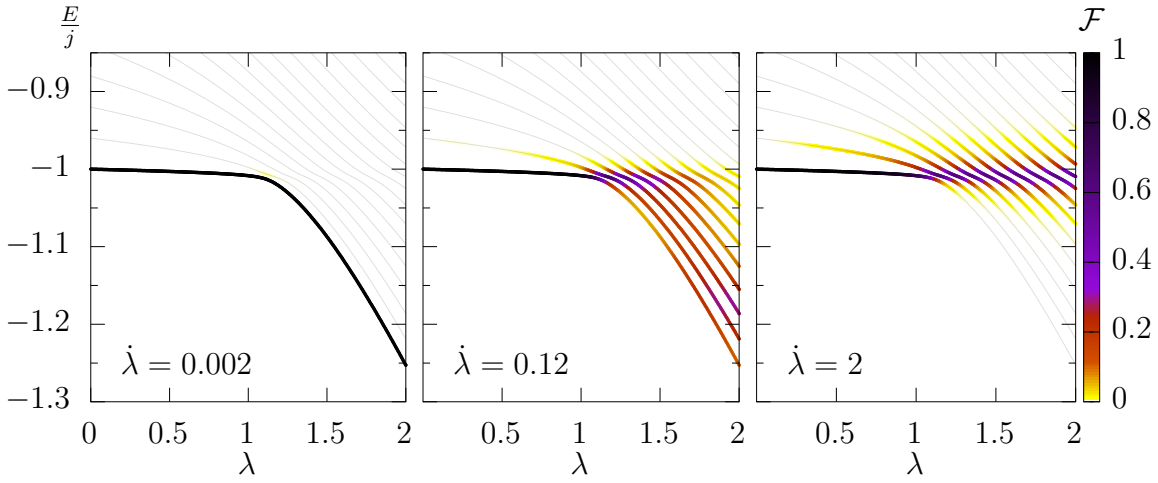

Figure 4.2: Instantaneous eigenstate fidelity $\mathcal{F}_k(t)$ as a function of time during an evolution induced directly by Hamiltonian $\hat{H}_2(\lambda)$ for $N = 100$ driven at various rates. The system starts in the ground state at $\lambda_\mathrm{i} = 0$, consequently only positive-parity subspace is populated. We don't depict negative-parity states.

4.2 Scaling of the ground-state population

4.2.1 Applicability of the Landau-Zener formula

The dependence of the final ground-state population on the driving rate $\dot{\lambda}$ and on the system size N is important for prospective applications in quantum adiabatic computing. Before inquiring into its study, it is worth reflecting on the applicability of the LZ formula (2.11). As the LZ problem deals with a two-level Hamiltonian, the comparison might make a good sense if the full LMG system starts in the ground state and when we assume that the ground state interacts practically exclusively with the first excited state (which has to be verified numerically).

However, there is a deeper difference in the objective of adiabatic quantum computing and of the LZ problem. In adiabatic quantum computing, the task usually is to get from a given λ_i to a given λ_f. The goal of the LZ problem is to cross the quantum critical point and to escape its effect on the system dynamics ($\lambda_\mathrm{f} \to \infty$).

Consequently, in our case, there exists a non-zero lower bound on the ground-state fidelity given by the diabatic limit. On the contrary, for the LZ case, no such lower bound exists and the ground-state fidelity can decrease arbitrarily close to zero. With this difference in mind, we will try nevertheless to compare our results (for $\dot{\lambda}$ smaller than some critical value) with the prediction of LZ formula in the following form

$$P_\mathrm{exc} \equiv 1 - \mathcal{F}_0(\tau) = \exp\left(-2\pi \frac{\Delta E^2}{4\alpha\dot{\lambda}}\right), \tag{4.1}$$

where P_exc denotes the excitation probability and $\mathcal{F}_0(\tau)$ the final ground-state fidelity.

Let us also comment a little on our more or less arbitrary choice of λ_f. For Hamiltonian $\hat{H}_1$ with a discontinuous QPT, the interaction of the ground state takes place almost only in the critical point (see fig. 4.3), therefore any choice

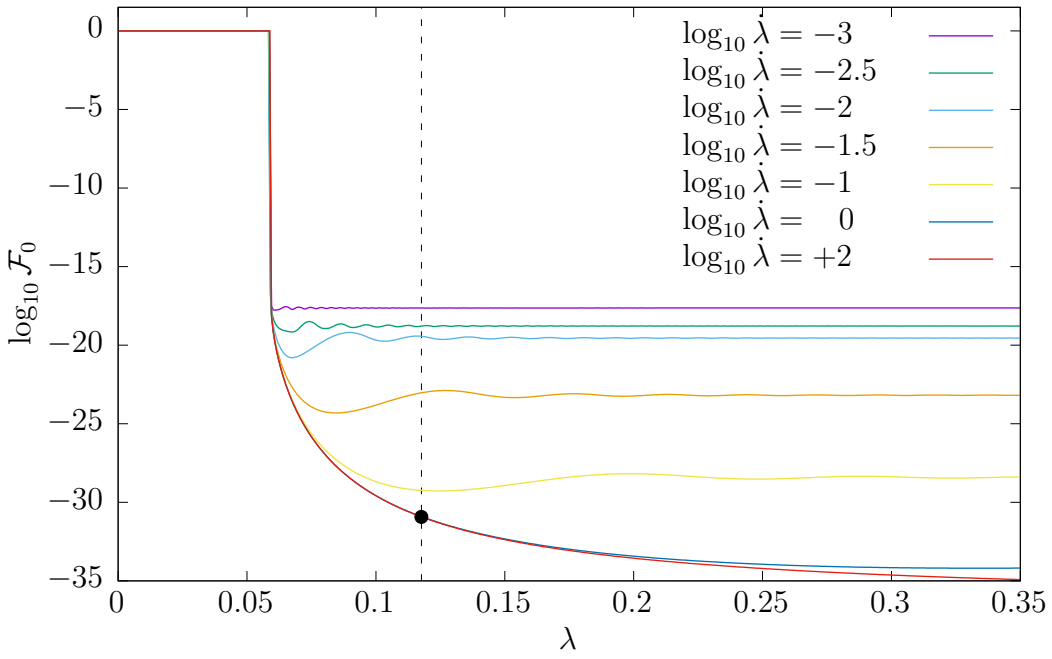

Figure 4.3: Instantaneous ground-state fidelity $\mathcal{F}_0$ as a function of control parameter $\lambda(t) = \dot{\lambda}t$ during an evolution induced directly by Hamiltonian $\hat{H}_1(\lambda)$ for system size $N = 20$ driven at various rates. The system starts in the ground state at $\lambda_\mathrm{i} = 0$. The vertical dashed line denotes $\lambda_\mathrm{f} = 2\lambda_\mathrm{c}$ and the black dot denotes the corresponding diabatic limit.

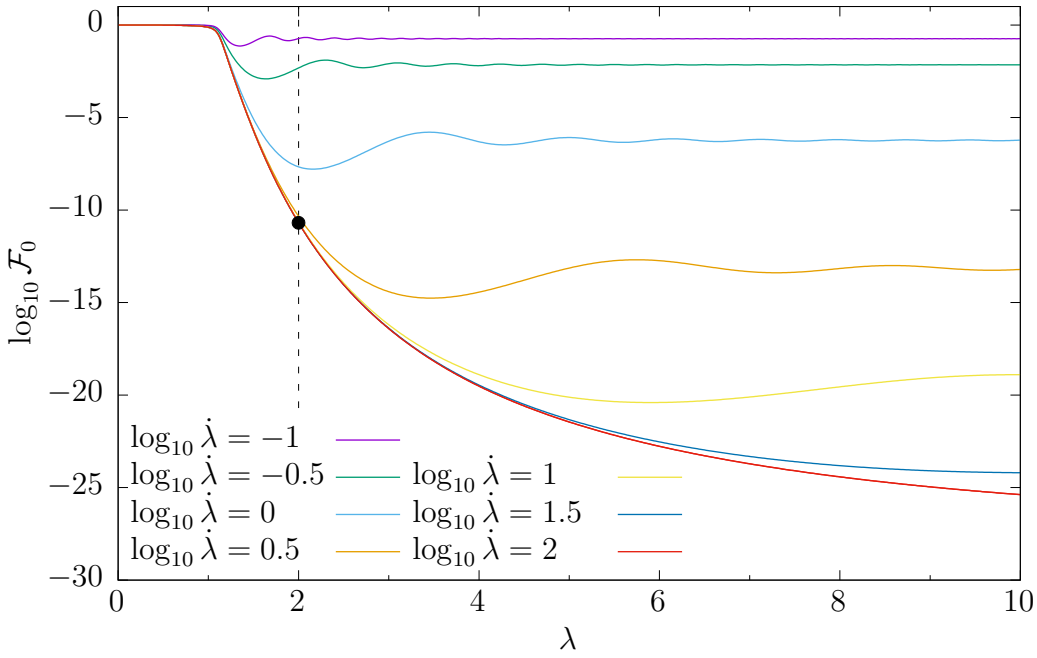

Figure 4.4: Instantaneous ground-state fidelity $\mathcal{F}_0$ as a function of control parameter $\lambda(t) = \dot{\lambda}t$ during an evolution induced directly by Hamiltonian $\hat{H}_2(\lambda)$ for system size $N = 100$ driven at various rates. The system starts in the ground state at $\lambda_\mathrm{i} = 0$. The vertical dashed line denotes $\lambda_\mathrm{f} = 2\lambda_\mathrm{c}$ and the black dot denotes the corresponding diabatic limit.

of λ_f is practically equivalent.

The situation is a bit more complex in the case of $\hat{H}_2$ with a continuous QPT. Figure 4.4 depicts how the ground-state population (fidelity) evolves as a function of λ. The curves corresponding to different values of $\dot{\lambda}$ are similar to each other. From a first glance it looks as if they were simply rescaled as a function of the driving parameter $\dot{\lambda}$ (including the magnitude and the period of oscillations and the stabilized value of $\mathcal{F}_0$). The oscillations can even begin well after $\lambda = 10$ for high driving rates.

Even though we don't have a reasonable extrinsic rule to set the value of λ_f, we can say that all the choices are qualitatively equivalent (the same evolution can be reached only with a different value of the driving rate).

4.2.2 Two-level approximation

To help interpret the results for the full LMG Hamiltonian, we will run some of the simulations also for a two-level approximative Hamiltonian in analogy with the LZ problem. This can be done for Hamiltonian $\hat{H}_1$ as the avoided crossings it comprises are asymptotically linear (even on the relatively small scales between individual avoided crossings). The main difference from the full $\hat{H}_1$ Hamiltonian is the absence of multilevel effects.

In this way, we can only approximate the evolution starting from the ground state (as the ground state undergoes only one avoided crossing). A unique two-level correspondence can be obtained by keeping the same approaching rate α, as defined in (2.10), and the same minimum distance ΔE. The corresponding two-level Hamiltonian reads

$$\hat{H}_1^{(\mathrm{2L})}(\lambda) = \begin{pmatrix} -j & \frac{1}{2}\Delta E(j) \\ \frac{1}{2}\Delta E(j) & \alpha(j)\cdot(\lambda_\mathrm{c}-\lambda) - j \end{pmatrix}, \tag{4.2}$$

where we denoted explicit dependence on the quasispin j. The minimum energy gap $\Delta E(j)$ is plotted in fig. 3.3 as a function of $N = 2j$. The value of the approaching rate can be determined from fig. 3.1 as $\alpha(j) \doteq 1.9215j/\lambda_\mathrm{c}$. The resulting spectrum of $\hat{H}_1^{(\mathrm{2L})}$ is plotted in fig. 4.5.

4.2.3 Landau-Zener region

To verify the applicability of the LZ formula (4.1) we first map the variables to linearize the dependence, in particular

$$\log_{10}\big(-\log P_\mathrm{exc}\big) = \log_{10}\frac{\pi}{2} + \log_{10}\frac{\Delta E^2}{\alpha} - \log_{10}\dot{\lambda}\,. \tag{4.3}$$

We kept together ΔE and α which both depend on the system size N. Since it is possible to adjust independently only $\dot{\lambda}$ and N, it doesn't make sense to separate also ΔE from α in the general case. Having reasoned that the LZ formula can hold only for processes with a certain range of the driving rate $\dot{\lambda}$, we begin with the dependence of the excitation probability on the driving rate.

We expect the validity of the LZ formula for Hamiltonian $\hat{H}_1$ due to the nature of its QPT. Truly, fig. 4.6 clearly consists of three regions – the LZ region (having the correct slope), the diabatic region (with a stabilized value of P_exc)

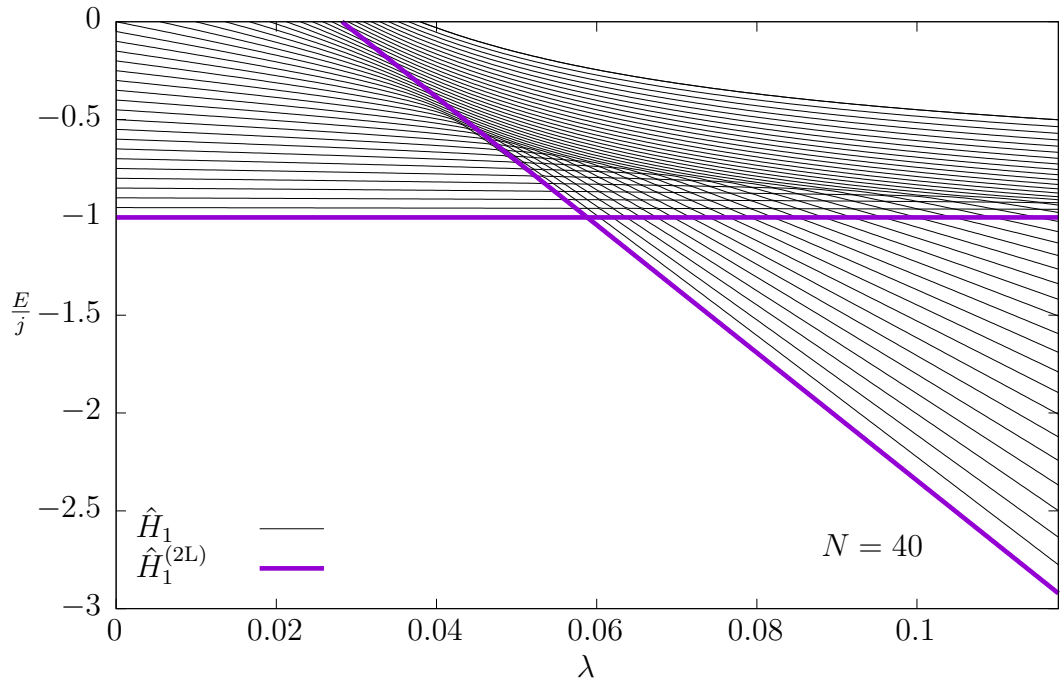

Figure 4.5: The spectrum of the corresponding two-level Hamiltonian $\hat{H}_1^{(2L)}(\lambda)$ compared with the spectrum of the original Hamiltonian $\hat{H}_1(\lambda)$.

and a transition between these two. A comparison with the corresponding two-level Hamiltonian (4.2) shows a total agreement in the LZ region. However, the stabilized value for the full Hamiltonian is lower than that for the two-level correspondence. We can conclude that this decrease in the ground-state population is due to the presence of multiple levels. Its consequence is an apparition of the transition region which is not present in the two-level case.

Notice that there are visible oscillations just before the transition to the stabilized diabatic value. This effect can be understood from fig. 4.3. For small values of $\dot{\lambda}$, the ground-state population doesn't fluctuate anymore at $\lambda = 2\lambda_c$ (the LZ region). For intermediary values of $\dot{\lambda}$, the ground-state population is still oscillating and the exact value is therefore shifted from the LZ value. The particular value of this shift strongly depends on the exact value of $\dot{\lambda}$. Finally, for $\dot{\lambda}$ high enough, the curves in fig. 4.3 don't differ anymore at $2\lambda_c$ (the diabatic region).

Figure 4.7 represents a similar figure for Hamiltonian $\hat{H}_2$. Since the avoided crossings are now continuous, there is no straightforward two-level LZ-like Hamiltonian. However, the plot manifests the same three regimes as for the Hamiltonian with a first-order QPT, i.e. the LZ regime, a transition and a diabatic regime.

As the minimum energy distance between the ground state and the first excited state (of the same parity) decreases only algebraically, the excitation probability is significantly lower than for $\hat{H}_1$. Therefore, the LZ region is approximately corresponding to $P_{\text{exc}} \in [0, 1/\text{e}]$, meaning that the ground-state population has to be higher than approximately 63%. Since obtaining such a high population is the goal of adiabatic quantum computing, we can say that in the interesting region of parameters, the LZ formula holds (so far) and we will hopefully be able to use it for making predictions for various values of $\dot{\lambda}$.

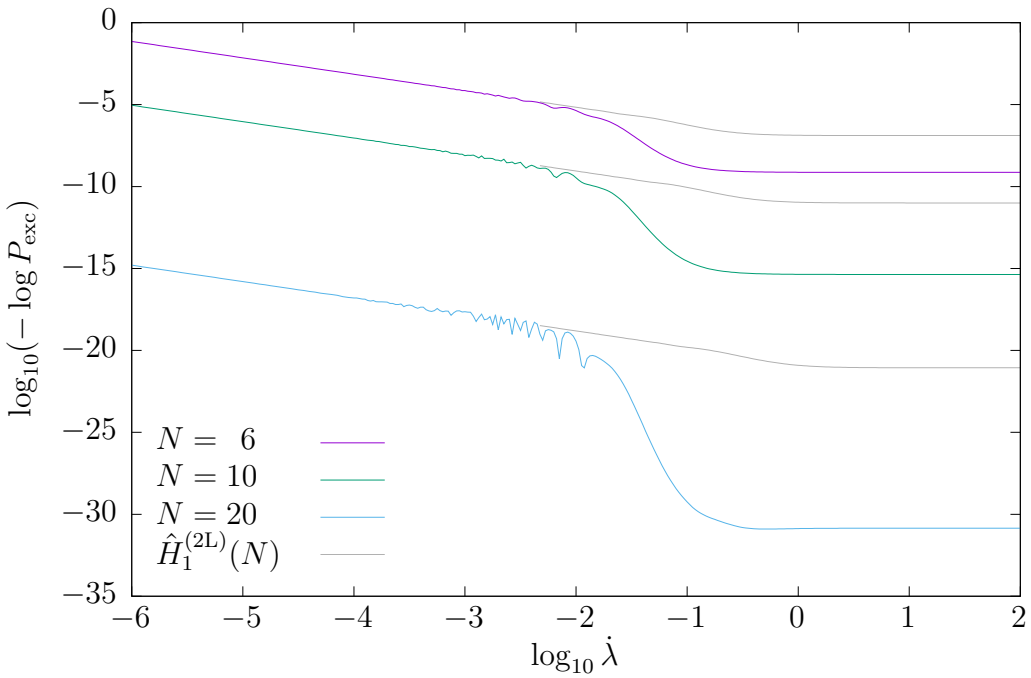

Figure 4.6: Dependence of the excitation probability $P_{\mathrm{exc}} = 1 - \mathcal{F}_0$ on the driving rate $\dot{\lambda}$ for Hamiltonian $\hat{H}_1$ with various values of system size N. Gray lines represent two-level approximation $\hat{H}_1^{(2\mathrm{L})}$ for the corresponding system sizes. Slow driving rates correspond with the LZ formula (slope -1). Notice that for $P_{\mathrm{exc}} \ll 1$ it holds $\log_{10}(-\log P_{\mathrm{exc}}) \approx \log_{10} \mathcal{F}_0$.

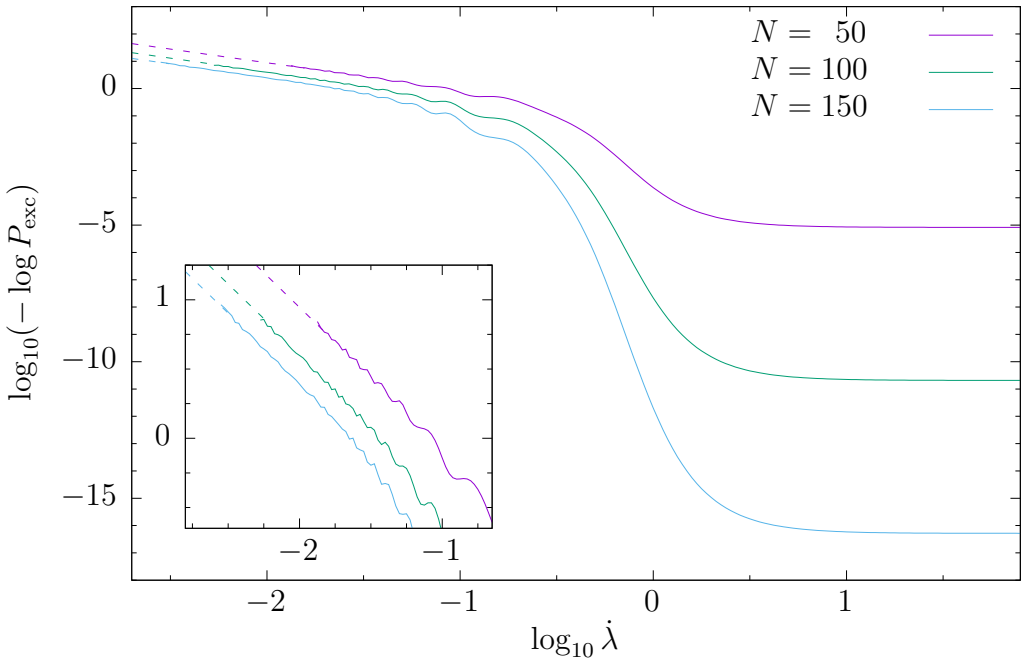

Figure 4.7: Dependence of the excitation probability $P_{\mathrm{exc}} = 1 - \mathcal{F}_0$ on the driving rate $\dot{\lambda}$ for Hamiltonian $\hat{H}_2$ with various values of system size N. Slow driving rates correspond with the LZ formula (slope -1). The dashed lines are a continuation based on the LZ formula, as numerical error prevails above certain $\mathcal{F}_0$. Notice that for $P_{\mathrm{exc}} \ll 1$ it holds $\log_{10}(-\log P_{\mathrm{exc}}) \approx \log_{10} \mathcal{F}_0$. The inset gives a detail on the LZ region.

4.2.4 Scaling with system size

For further study of the ground-state population scaling with the system size, we will restrict the possible values of $\dot{\lambda}$ on the LZ region corresponding to each particular system size. Since we already established the validity of the LZ formula for $\dot{\lambda}$, we will devise a new variable suitable for studying scaling with N, that being

$$\log_{10} y \equiv \log_{10}\Big(-\dot{\lambda}\log P_{\text{exc}}\Big) = \log_{10}\frac{\pi}{2} + \log_{10}\frac{\Delta E^2}{\alpha}\,. \tag{4.4}$$

Based on this form of the LZ formula, we will also devise particular functions of N with which we will fit the data. We already know that ΔE scales exponentially or algebraically with N for $\hat{H}_1$ or $\hat{H}_2$, respectively (see fig. 3.3). Remember also that $\alpha_1(N) \doteq 1.9215N/2\lambda_{\text{c}}$ for Hamiltonian $\hat{H}_1$. On the other hand for $\hat{H}_2$, there is no such thing as α_2 because the interacting-phase ground-state energy is not linear in λ. We can however make an assumption that an effective value of α_2 exists and instead of being linear in N, we will let it be a general power N^{ξ}. This will, hopefully, reflect the continuous nature of the QPT. Putting this information together, the final form of the LZ-based fitting functions is

$$\log_{10} y_1(N) = a_1 N - \log_{10} N + c_1\,, \tag{4.5}$$

$$\log_{10} y_2(N) = b_2 \log_{10} N + c_2\,. \tag{4.6}$$

Figures 4.8 and 4.9 successfully verified the validity of the LZ formula for both Hamiltonians. All data points for different values of $\dot{\lambda}$ truly lie on a single curve which is correctly fitted by the LZ-based fitting functions. We can go further in this examination for Hamiltonian $\hat{H}_1$ and compare the fitted values $a_1 = -0.938(2)$, $c_1 = -0.72(3)$ with those computed from $\Delta E_1(N)$ fit. These values roughly correspond (the leading term is $a_1' = -1.005(1)$) but don't give a satisfying match. The discrepancy comes from the deviation of the true $\Delta E_1(N)$ from the fitted exponential function.

To overcome this difficulty, we used the true values of ΔE and fitted only the constant factor $\pi/2$ in the LZ formula (4.4). This time we obtained $k \cdot \pi/2$ where $k = 1.05(3)$, i.e. a very good correspondence with the LZ formula. Figure 4.8 contains a comparison with the exact LZ formula (for which $k = 1$).

The datapoints in fig. 4.9 have a slightly bigger fluctuation around the LZ-based fit, nevertheless, all of them clearly lie on a single curve. Consequently, a variant of the LZ formula holds in this case, too. We can infer how the effective value of α_2 scales with the system size from the fitted coefficients $b_2 = -1.19(1)$, $c_2 = 0.97(2)$ and from $\Delta E_2(N)$ fit, in particular $\alpha_2(N) = \bar{\alpha}_2 N^{\xi}$ where $\xi = 0.47(1)$ and $\bar{\alpha}_2 = 0.52(4)$.

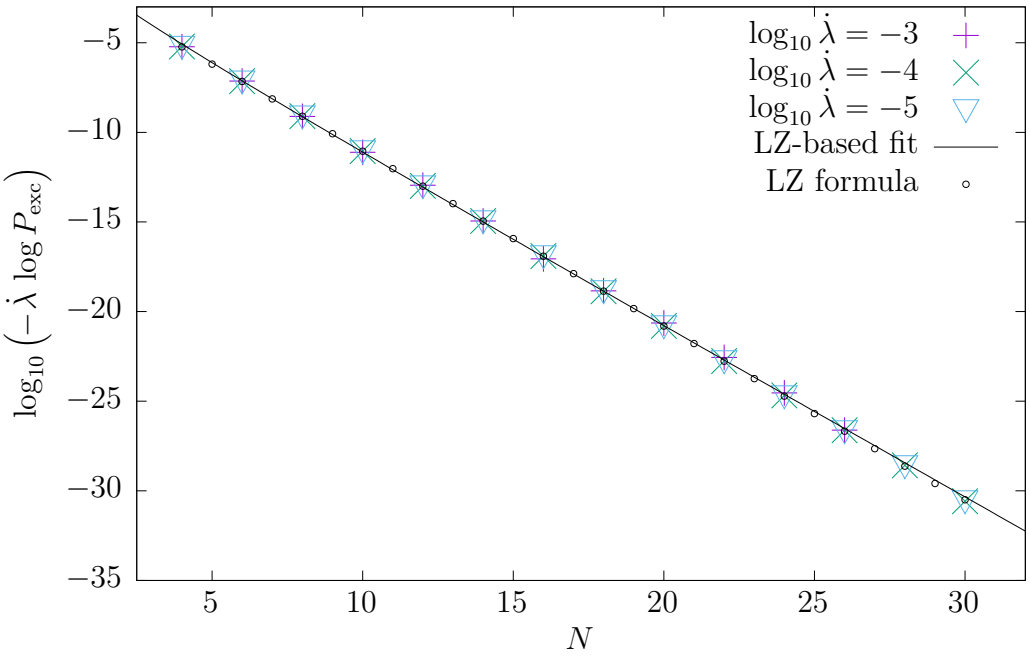

Figure 4.8: Verification of the LZ formula for Hamiltonian $\hat{H}_1$ within the range of $\dot{\lambda}$ values corresponding to the LZ region (the left half of fig. 4.6). The graph shows how a relevant quantity constructed from the driving rate $\dot{\lambda}$ scales with the system size N.

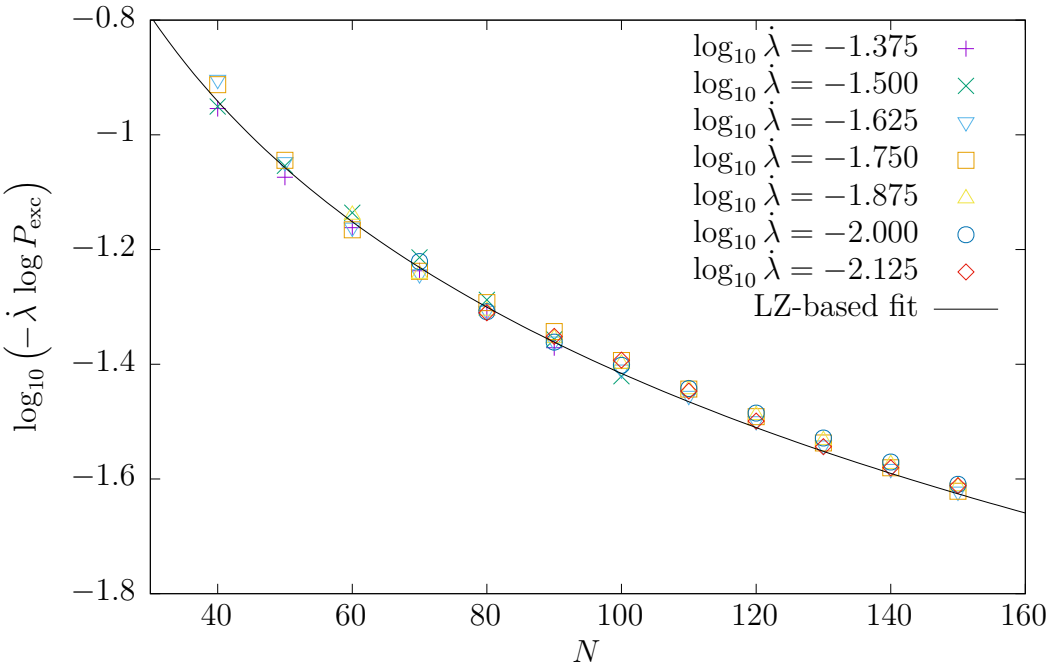

Figure 4.9: Verification of the (modified) LZ formula for Hamiltonian $\hat{H}_2$ within the range of $\dot{\lambda}$ values corresponding to the LZ region (as in the inset of fig. 4.7). The graph shows how a relevant quantity constructed from the driving rate $\dot{\lambda}$ scales with the system size N.

4.2.5 Adiabatic driving rate

Let us define $\mathcal{F}_0 = \text{const}$ a value we wish to obtain at the end of the external driving procedure. Of interest is a high enough value $\mathcal{F}_0$ in order to be able to identify correctly the solution of an adiabatic quantum computation. The question is how slowly we need to drive our system (depending on the system size) in order to obtain the desired ground-state population (e.g. $\mathcal{F}_0 = 0.9$, or equivalently $P_{\text{exc}} = 0.1$). This information is a simple result of the previous analysis. Within the LZ region, it holds for the *adiabatic driving rate*

$$\dot{\lambda}^{\text{A}}(N) = -\frac{\pi}{2\log P_{\text{exc}}}\frac{\Delta E^2(N)}{\alpha(N)} = \frac{y(N)}{-\log P_{\text{exc}}}\,. \tag{4.7}$$

Now, we immediately see, that $\dot{\lambda}^{A}(N)$ for $\hat{H}_1$ decreases exponentially, whereas for $\hat{H}_2$ only algebraically,

$$\dot{\lambda}_1^{\text{A}}(N) \sim \frac{1}{N\mathrm{e}^{2.160\,N}}\,, \tag{4.8}$$

$$\dot{\lambda}_2^{\text{A}}(N) \sim \frac{1}{N^{1.19}}\,. \tag{4.9}$$

This makes a significant difference in practice. Acquiring an adiabatic passage through a QPT of the second order (continuous QPTs in general) is possible simply by driving the control parameter λ slowly enough. On the other hand, if we wanted an adiabatic passage through a QPT of the first order, we would need to employ an adibatic shortcut.

4.3 Non-zero temperature

Before we delve into adiabatic shortcuts, we will investigate the effect of non-zero temperature on the final ground-state population. At non-zero temperature, the ground-state dynamics gets mixed with the dynamics of excited states. A few examples of the system evolution starting from the energetically lowest states are depicted in figs. 4.10 and 4.11. We see that, sometimes, the evolution starting from an excited state can possibly produce higher ground-state fidelity in the end. This is caused by the fact that avoided crossings in excited states aren't as strong as the avoided crossing of the ground-state.

An interesting result for the ground-state fidelity holds in the limit of infinite temperature. All initial eigenstates are populated equally, that is $p_n = 1/\dim\mathcal{H}$, where $\mathcal{H}$ denotes the Hilbert space. Equation (2.29) can then be rewritten as follows

$$\mathcal{F}_0(\tau) = \frac{1}{\dim\mathcal{H}}\sum_n \left|\left\langle 0(\tau)\middle|\hat{U}\middle|n(0)\right\rangle\right|^2 = \frac{1}{\dim\mathcal{H}}\,, \tag{4.10}$$

where we used the fact that vectors $\hat{U}\,|n(0)\rangle$ form a basis of Hilbert space $\mathcal{H}$. The remaining sum then simply represents squared projections of vector $\langle 0(\tau)|$ onto each basis vector which add up to 1. By the same logic, it holds $\mathcal{F}_k(t) = 1/\dim\mathcal{H}$ for a general k-th eigenstate fidelity.

This value of fidelity doesn't depend on the driving rate (or time τ of the transition) at all. Therefore, for a sufficiently high temperature, carrying out an

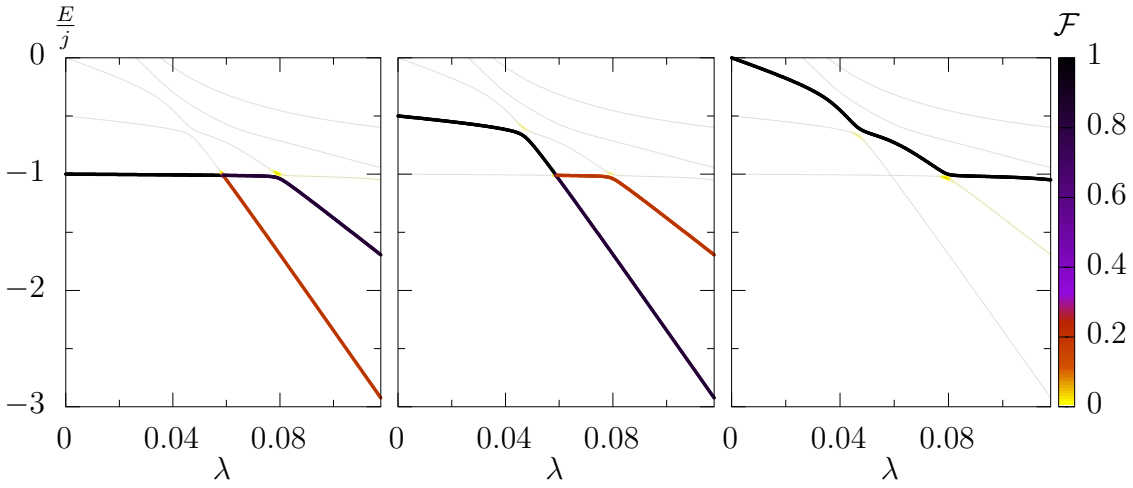

Figure 4.10: Instantaneous eigenstate fidelity $\mathcal{F}_k(t)$ as a function of time during an evolution induced directly by Hamiltonian $\hat{H}_1(\lambda)$ for $N = 4$ driven at rate $\log_{10} \dot{\lambda} = -4.5$. The system starts in various instantaneous eigenstates.

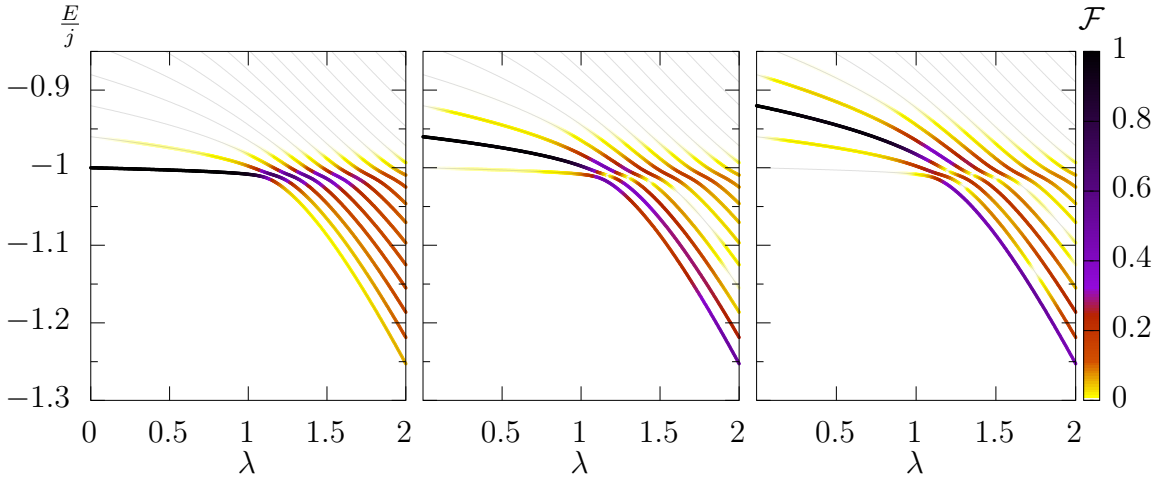

Figure 4.11: Instantaneous eigenstate fidelity $\mathcal{F}_k(t)$ as a function of time during an evolution induced directly by Hamiltonian $\hat{H}_2(\lambda)$ for $N = 100$ driven at rate $\dot{\lambda} = 0.2$. The system starts in various instantaneous eigenstates.

adiabatic passage is a waste of time and resources as one would obtain the exact same result even with an instantaneous change straight to the final Hamiltonian. Also $1/\dim \mathcal{H}$ is typically much higher than the original diabatic limit for zero temperature, hence high temperature raises the diabatic limit in figs. 4.6 and 4.7.

4.3.1 Thermal state dynamics

Once again for numerical reasons, we will demonstrate the system dynamics for $\hat{H}_1$ as a function of the system size and for $\hat{H}_2$ as a function of the driving rate. We have already seen, while investigating the LZ formula, that both these parameters can have a similar impact on the system dynamics. The difference is only in the strength of this dependence and on the region of values that we are able to probe numerically.

Given that the evolution of $\hat{H}_2$ conserves parity subspaces, we can restrict ourselves on the case of a thermal reservoir which conserves the same parity. The

situation remains qualitatively the same as the only difference is the initial redistribution of population among individual eigenstates (due to a different energy spacing and a different number of states in the given parity subspace).

Figures 4.12 and 4.13 depict the evolution of instantaneous eigenstate fidelity in analogy with the ground-state case in figs. 4.10 and 4.11. The figures depict a boost in $\mathcal{F}_0$ of two kinds. One corresponds to a low temperature and it visibly makes use of wider energy gaps in the excited spectrum to directly maximize the ground-state fidelity. The second type of boost corresponds to quite a high temperature causing a nearly uniform redistribution of states resulting in eq. (4.10).

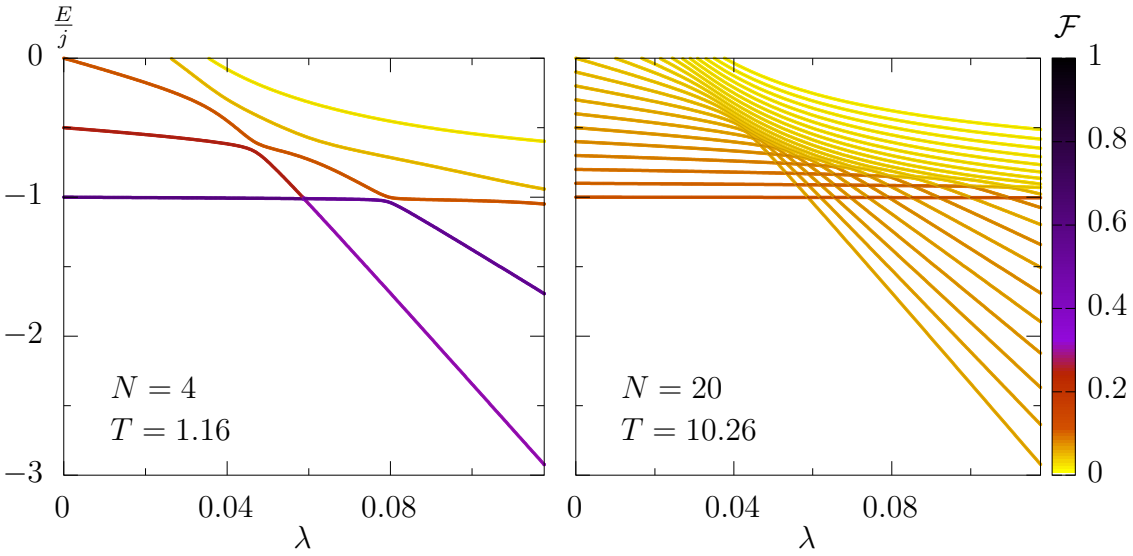

Figure 4.12: Instantaneous eigenstate fidelity $\mathcal{F}_k(t)$ as a function of time during an evolution induced directly by Hamiltonian $\hat{H}_1(\lambda)$ for two different system sizes driven at $\log_{10}\dot{\lambda} = -4.5$. The system starts in a thermal state at $\lambda_\mathrm{i} = 0$ and at temperature T chosen to maximize $\mathcal{F}_0$.

The whole dependence of $\mathcal{F}_0$ on the temperature is shown in figs. 4.14 and 4.15. There are three possible ways in which the temperature can affect the ground-state fidelity. If the zero-temperature $\mathcal{F}_0$ is greater than the high-temperature limit (4.10), then there is a step-wise decrease of the groud-state fidelity starting from a certain critical value of temperature. If the zero-temperature fidelity is comparable to the high-temperature limit, then a clear maximum of $\mathcal{F}_0$ arises at an optimum value of temperature. At last, if the zero-temperature value is considerably lower than the high-temperature one, there is a step-wise growth at a certain critical temperature. This analysis applies to both Hamiltonians.

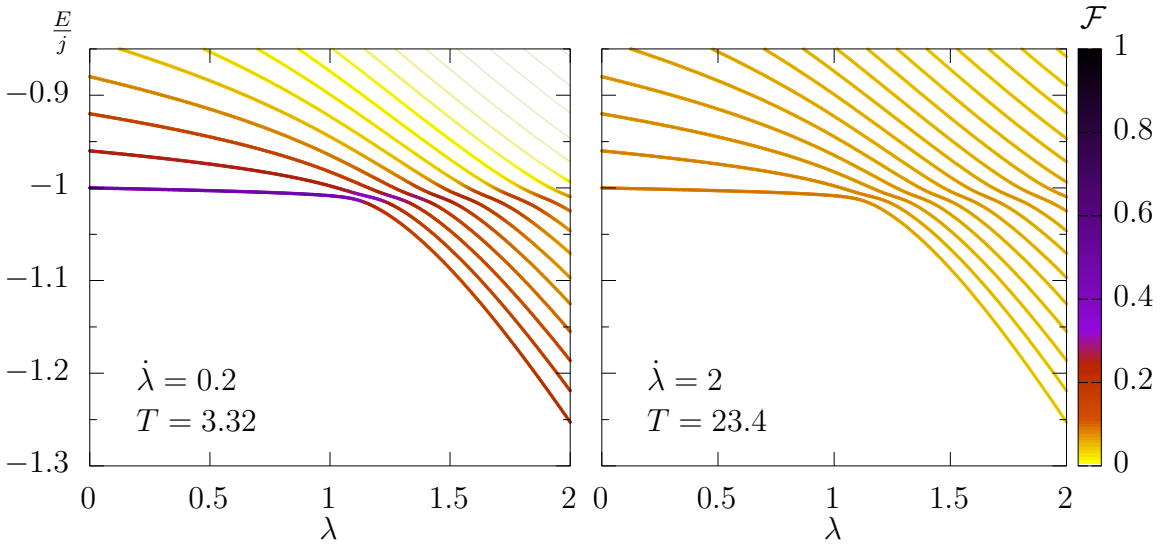

Figure 4.13: Instantaneous eigenstate fidelity $\mathcal{F}_k(t)$ as a function of time during an evolution induced directly by Hamiltonian $\hat{H}_2(\lambda)$ for $N = 100$ driven at two different rates. The system starts in a thermal state at $\lambda_\mathrm{i} = 0$ and at temperature T chosen to maximize $\mathcal{F}_0$. We don't depict negative-parity states.

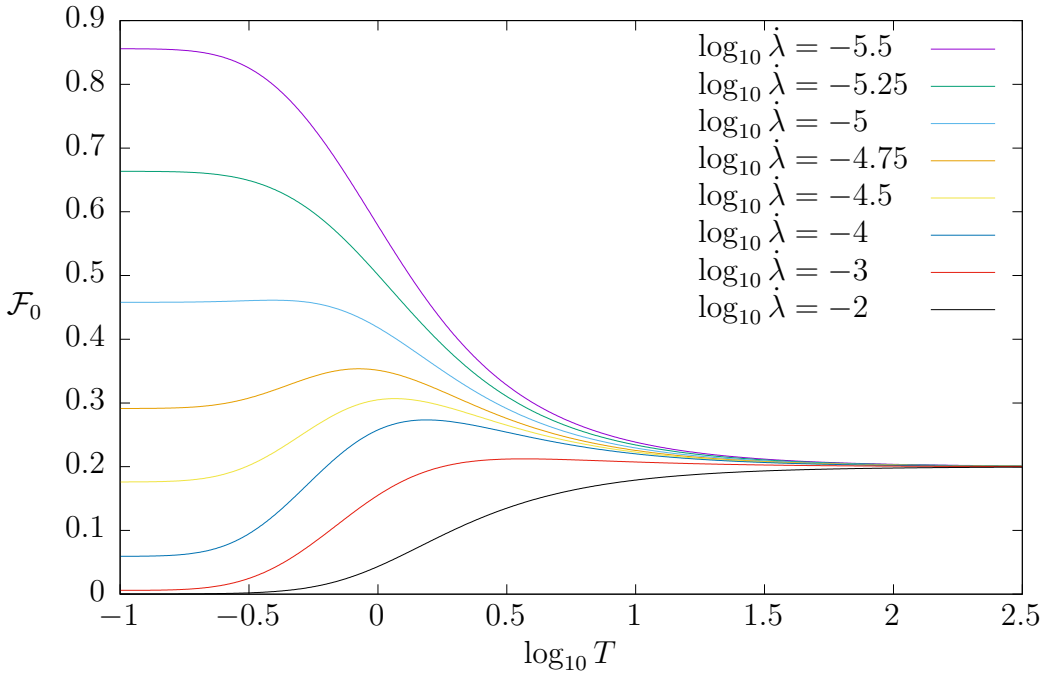

Figure 4.14: The dependence of ground-state fidelity $\mathcal{F}_0$ on temperature T for Hamiltonian $\hat{H}_1$ and system size $N = 4$.

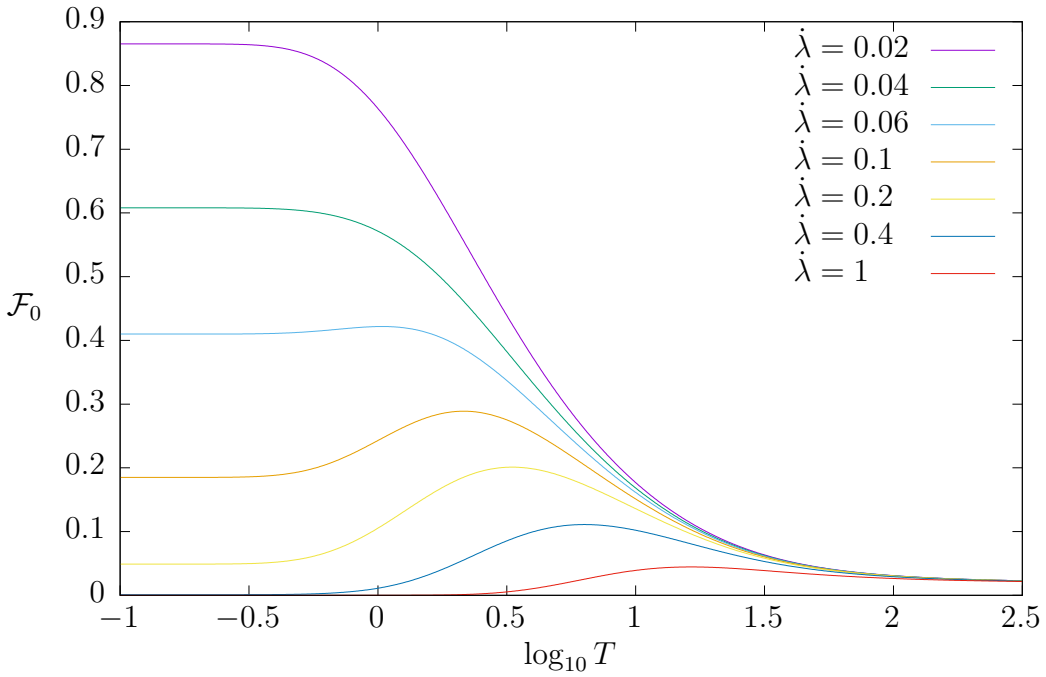

Figure 4.15: The dependence of ground-state fidelity $\mathcal{F}_0$ on temperature T for Hamiltonian $\hat{H}_2$ and system size $N = 100$.

4.3.2 Optimum temperature

It is possible to choose an optimum value of temperature to maximize the resulting ground-state fidelity. Figure 4.16 depicts the dependence of such an optimal fidelity on the driving rate for Hamiltonian $\hat{H}_2$. Notice that black and partly also violet points correspond practically to the ground-state evolution (zero temperature). Therefore the oscillations in $\mathcal{F}_0$ are not an effect of temperature optimization. On the contrary, they are the same oscillations as in fig. 4.7 (be careful about comparing the logarithmic and linear scale of $\dot{\lambda}$). The upper half of the figure also roughly corresponds to the LZ region ($\mathcal{F}_0 \gtrsim 0.63$).

A similar graph of the optimal fidelity for $\hat{H}_1$ is shown in fig. 4.17. Due to the exponential scaling with N, a common case scenario for $\hat{H}_1$ is that the system is found close to the limit given by (4.10) over a wide range of driving rates. The only exception are very slowly driven very small systems (such as $N = 4$ and $\log_{10} \dot{\lambda} \sim -5.5$).

In conclusion, the effect of temperature can actually boost the final ground-state fidelity. In practice, this case is of little significance to adiabatic quantum computing as one aims to obtain as high fidelity as possible. Therefore, adiabatic quantum computers will have to be cooled down below a certain critical temperature to be able to obtain for instance $\mathcal{F}_0 \sim 0.9$.

In theory, if combined with classical computers, high-temperature adiabatic quantum computing could be used to find solutions to NP problems [55, 56], provided that the dimension of the Hilbert space is kept reasonably low. The principle is that a repeated execution of adiabatic quantum computing will result in a set of possible solutions (as we don't know which measurement corresponds to the ground-state solution). Therefore, if we are able to "easily" check if a given candidate solution is a true solution (the definition of an NP problem), we could

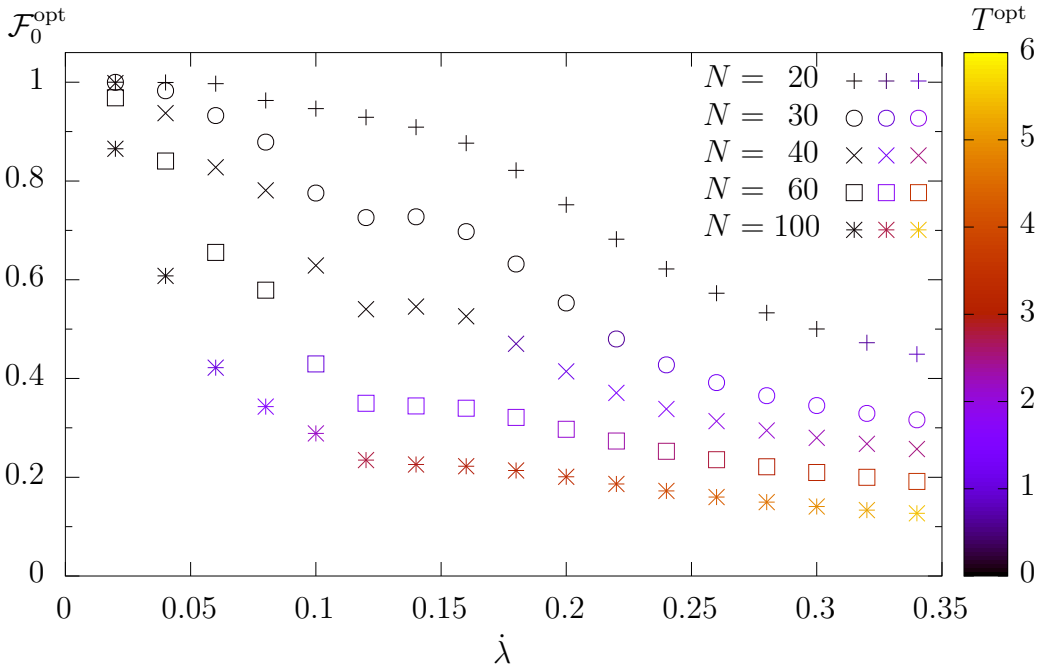

Figure 4.16: The dependence of optimum ground-state fidelity $\mathcal{F}_0^{\text{opt}}$ on driving rate $\dot{\lambda}$ for Hamiltonian $\hat{H}_2$. The colour scale depicts the corresponding optimum temperature T^{opt}.

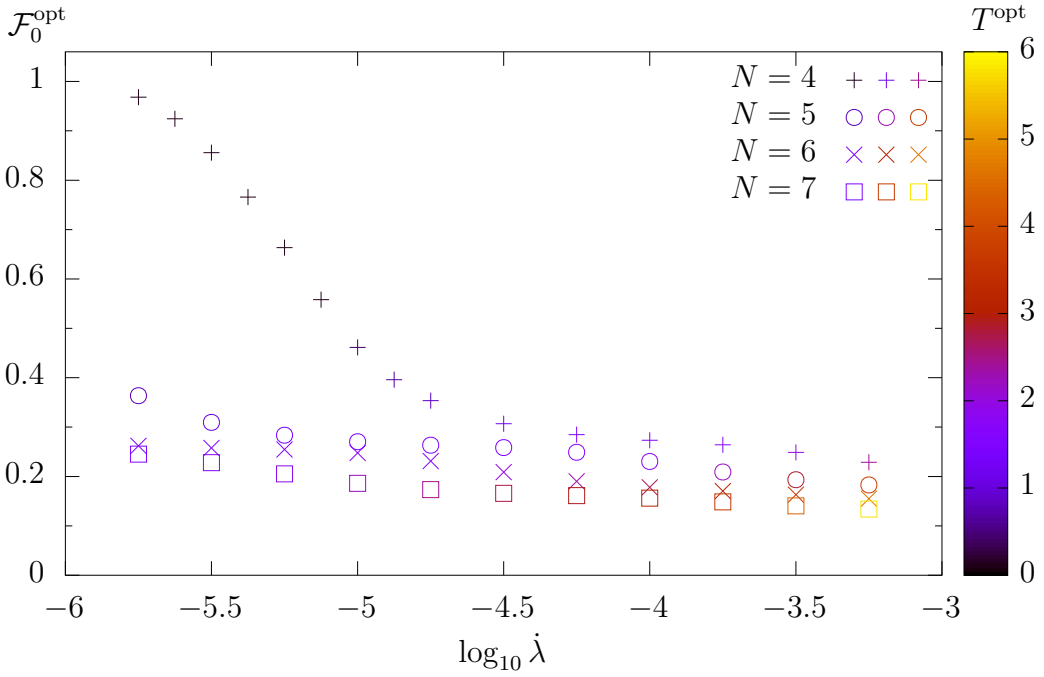

Figure 4.17: The dependence of optimum ground-state fidelity $\mathcal{F}_0^{\text{opt}}$ on driving rate $\dot{\lambda}$ for Hamiltonian $\hat{H}_1$. The colour scale depicts the corresponding optimum temperature T^{opt}.

simply pick the correct solution from all the possible candidates whose number is at most $\dim \mathcal{H}$. The bottleneck of this approach is that $\dim \mathcal{H}$ itself grows exponentially with the number of degrees of freedom of the adiabatic quantum computer. Only, it is quite safe to assume that problems of practical interest will require a considerably large adiabatic quantum computers (with a high number of degrees of freedom).

5. Counter-diabatic driving

5.1 System dynamics

Let us now turn to a guaranteed way to obtain 100% ground-state fidelity of the final Hamiltonian. This is achieved with the use of counter-diabatic driving (adiabatic shortcuts). Figure 5.1 gives an example of such an evolution. The case of $\hat{H}_2$ corresponds exactly to the last subfigure in fig. 4.2. The counter-diabatic evolution of $\hat{H}_1$ can be compared with the middle subfigure in fig. 4.1 which was driven even more slowly and yet resulted in almost no population of the ground state.

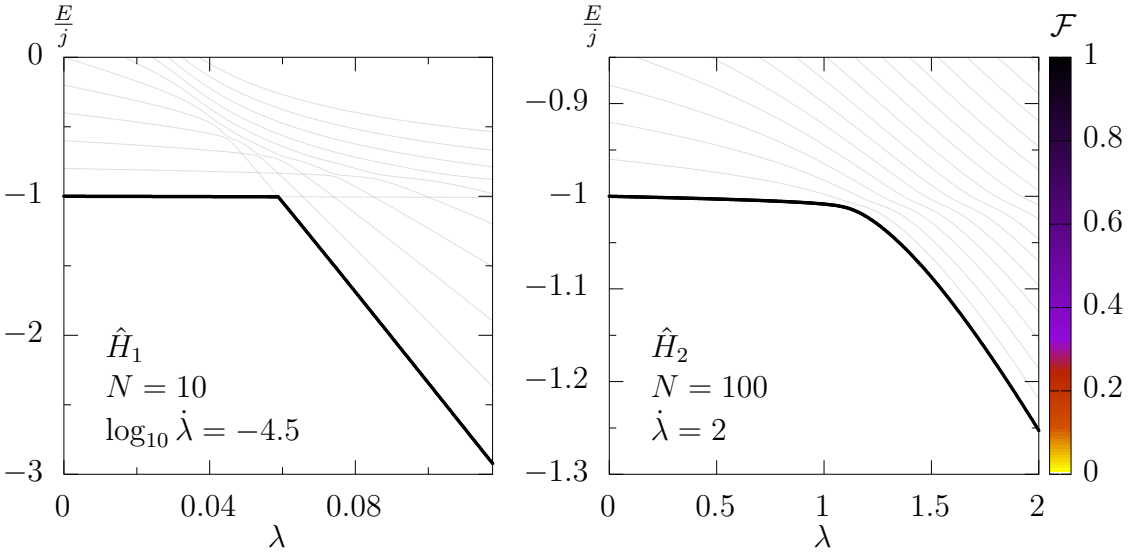

Figure 5.1: Instantaneous eigenstate fidelity $\mathcal{F}_k(t)$ as a function of time during a counter-diabatic driving corresponding to Hamiltonians $\hat{H}_1(\lambda)$ and $\hat{H}_2(\lambda)$ for one chosen system size N and one driving rate $\dot{\lambda}$. The system starts in the ground state at $\lambda_\mathrm{i} = 0$.

5.2 Shortcut cost

We demonstrated that adiabatic shortcuts work well even in the presence of QPTs and ESQPTs. But there is another very important aspect, and that is how difficult or how costly it is to employ such a shortcut. Figure 5.2 shows the evolution of the transition matrix element during the external driving procedure. A very sharp and very high peak is found at the QPT of the first order. For the continuous QPT a distinct peak arises as well, albeit not nearly as sharp as for $\hat{H}_1$. Comparing fig. 5.2 with fig. 3.3, one sees that the maximum value of $\mathcal{M}$ is a bit greater than $1/\Delta E$ in agreement with (2.15).

The integrated cost $\mathcal{C}$ of adiabatic shortcuts is proportional to the first power of the driving rate $\dot{\lambda}$ as a general theoretical result. It remains only to study the scaling of the adiabatic shortcut cost with the system size N for a fixed value of $\dot{\lambda}$. This dependence, as shown in fig. 5.3, is once again found to scale exponentially with the system size for $\hat{H}_1$ and algebraically for $\hat{H}_2$.

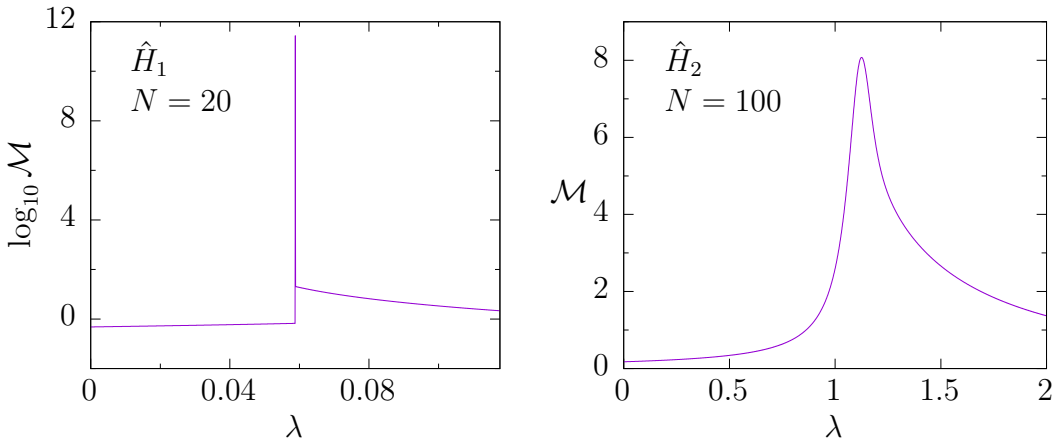

Figure 5.2: Transition matrix element $\mathcal{M}$ for driving rate $\dot{\lambda} = 1$ as a function of control parameter λ for Hamiltonians $\hat{H}_1$ and $\hat{H}_2$. Notice the logarithmic axis for $\hat{H}_1$ and linear axis for $\hat{H}_2$.

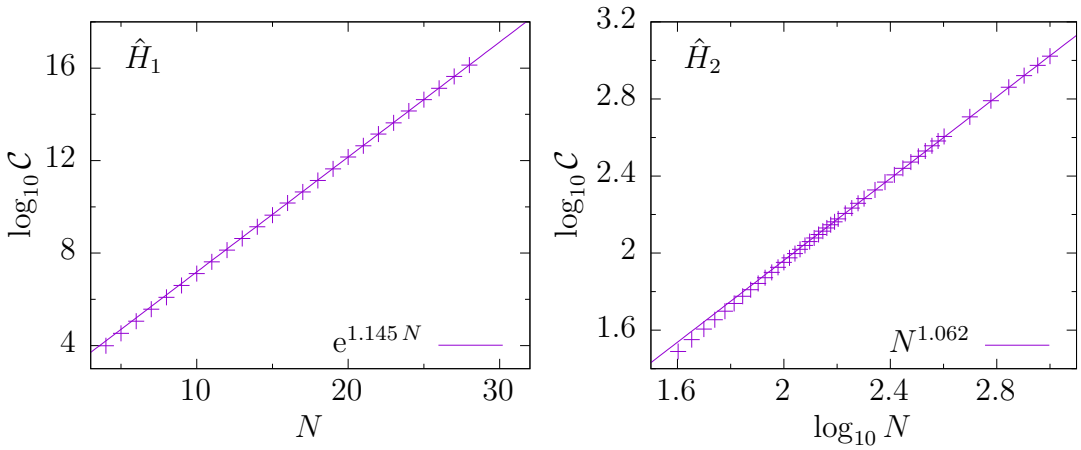

Figure 5.3: Scaling of the adiabatic shortcut cost $\mathcal{C}$ with system size N for Hamiltonians $\hat{H}_1$ and $\hat{H}_2$ driven at rate $\dot{\lambda} = 1$. The dependence is fitted by an exponential and a power function, respectively.

To summarize, it is possible to avoid the usage of adiabatic shortcuts for $\hat{H}_2$ simply by driving $\hat{H}_2(\lambda)$ slowly enough. However, if we wanted to arrive at the correct result faster, it would be possible to employ an adiabatic shortcut as its cost grows practically only linearly with the system size. On the other hand, the manipulation of $\hat{H}_1$ is way more demanding. To obtain a high ground-state fidelity, one has to employ an adiabatic shortcut. On top of that, their cost grows exponentially with system size. Therefore such adiabatic shortcuts might even turn out too expensive to perform them at all.

Conclusion

We verified numerically the validity of the adiabatic approximation in the presence of QPTs and ESQPTs in the LMG model. The time period τ of the transition between the initial and final value of the control parameter λ which is needed for a practically adiabatic passage depends on the minimum gap in the energy spectrum throughout the external driving procedure. This minimum gap ΔE decreases exponentially in system size N for a Hamiltonian with a discontinuous QPT and algebraically for a Hamiltonian with a continuous QPT. In agreement with this dependence, also the time period τ needed for adiabaticity grows exponentially in N for Hamiltonian $\hat{H}_1$ and algebraically for $\hat{H}_2$. This allows for obtaining high ground-state population for systems without any QPT or with a continuous QPT. On the other hand, to obtain the same results for systems with a discontinuous QPT, one has to employ an adiabatic shortcut.

We studied in detail the dependence of the final ground-state population P_0 on the driving rate $\dot{\lambda}$ (proportional to τ^{-1}). There are three major regimes based on the dependence of P_0 on the driving rate. For a very slow driving, the full system obeys the LZ formula (derived for an avoided crossing corresponding to a discontinuous QPT in two-level systems). In contrast, for a fast driving, the ground-state population doesn't depend on $\dot{\lambda}$ as it already reached the diabatic limit. There is a transition between these two regimes for intermediary values of $\dot{\lambda}$. The transition manifests oscillatory behaviour and its presence is an effect of multiple energy levels. These results hold for both Hamiltonians $\hat{H}_1$ and $\hat{H}_2$.

Since we are interested in high ground-state populations, we can restrict ourselves only on the region compliant with the LZ formula. We investigated the scaling of P_0 with the system size N in this region. It is straightforward to compare results for $\hat{H}_1$ with the LZ formula as both describe a discontinuous QPT. The ground-state population in $\hat{H}_1$ satisfies rather exactly the prediction of the LZ formula. Such an analogy for Hamiltonian $\hat{H}_2$ is more difficult. We, nonetheless, succeeded in identifying the formula obeyed by P_0. This allowed us to define an effective form of the LZ formula also for Hamiltonian $\hat{H}_2$.

Achieving a true zero temperature is not possible in practice, hence we are interested also in the effect of non-zero temperature on the performance of adiabatic quantum computers. We made a first step in this direction by considering the initial system in equilibrium with a thermal reservoir at temperature T. The system is then separated from the reservoir and it undergoes the external driving starting from the statistical mixture of states induced by the thermal reservoir. One effect of non-zero temperature is that the diabatic limit can be significantly increased by optimizing the temperature of the reservoir. The dependence of the ground-state population on the initial temperature can be either a step-like function (both decreasing or increasing) or it can exhibit a definite peak at a certain temperature. The case important for adiabatic quantum computing (i.e. a high ground-state population) corresponds, however, to a decreasing step-like function. Therefore, there is a certain critical temperature below which one needs to cool the system down. In summary, only a little practical advantage can be gained from a non-zero temperature.

We demonstrated numerically a successful counter-diabatic driving procedure

for both Hamiltonians $\hat{H}_1$ and $\hat{H}_2$. Having defined a suitable measure for the difficulty of implementing an adiabatic shortcut, we found that the adiabatic shortcut cost $\mathcal{C}$ grows exponentially with system size N for Hamiltonian $\hat{H}_1$ and only algebraically for $\hat{H}_2$. This allows for the use of counter-diabatic driving once again only for systems without any QPT or with a continuous QPT. Counter-diabatic driving through a discontinuous QPT would probably be too "expensive" to execute.

A. No-crossing theorem

For the reader's convenience we present the same technique of formulating and proving the no-crossing theorem which we already presented in [52] which itself was a more detailed analysis of a proof published in [57].

Consider Hamiltonian $\hat{H}(\lambda)$ which depends on a single real parameter λ and denote $\mathfrak{p}(\lambda, E)$ its characteristic polynomial,

$$\mathfrak{p}(\lambda, E) = \det\Big(\hat{H}(\lambda) - E\Big)\,. \tag{A.1}$$

Each eigenenergy $E_k(\lambda)$ of Hamiltonian $\hat{H}(\lambda)$ by definition satisfies

$$\mathfrak{p}(\lambda, E_k(\lambda)) = 0\,. \tag{A.2}$$

Now suppose a real crossing between $E_i(\lambda)$ and $E_j(\lambda)$ at $\lambda = \Lambda$ and denote ε the energy of the crossing, i.e. $\varepsilon = E_i(\Lambda) = E_j(\Lambda)$. We examine *crossings* of energy levels and so we suppose $E_i(\lambda) \neq E_j(\lambda)$ in a deleted neighbourhood of Λ.

Because ε represents a *real* crossing, it has to be a double root of $\mathfrak{p}(\Lambda, E)$. Mathematically written,

$$\mathfrak{p}(\Lambda, \varepsilon) = 0\,, \tag{A.3}$$

$$\frac{\partial \mathfrak{p}}{\partial E}(\Lambda, \varepsilon) = 0\,. \tag{A.4}$$

Equation (A.2) has to hold for each λ along any energy level $E_k(\lambda)$, that is, in particular for $k \in \{i, j\}$ and for $\lambda = \Lambda + \delta\lambda$ close to Λ,

$$\begin{aligned} 0 = \mathfrak{p}\Big(\lambda, E_k(\lambda)\Big) \approx \\ \approx \underbrace{\mathfrak{p}(\Lambda, \varepsilon)}_{0} + \frac{\mathrm{d}}{\mathrm{d}\lambda}\Big[\mathfrak{p}\Big(\lambda, E_k(\lambda)\Big)\Big]\Big|_{\Lambda,\varepsilon} \delta\lambda = \\ = \left(\frac{\partial \mathfrak{p}}{\partial \lambda}(\Lambda, \varepsilon) + \underbrace{\frac{\partial \mathfrak{p}}{\partial E}(\Lambda, \varepsilon)}_{0} \frac{\mathrm{d}E_k}{\mathrm{d}\lambda}(\Lambda)\right) \delta\lambda = \\ = \frac{\partial \mathfrak{p}}{\partial \lambda}(\Lambda, \varepsilon)\delta\lambda\,. \end{aligned} \tag{A.5}$$

Thus, we obtained another independent condition for a real energy crossing,

$$\frac{\partial \mathfrak{p}}{\partial \lambda}(\Lambda, \varepsilon) = 0\,. \tag{A.6}$$

In order for a real energy crossing to occur, the roots of characteristic polynomial $\mathfrak{p}(\lambda, E)$ would have to satisfy two independent conditions (A.4), (A.6) at the same time. Put another way, unless there is a very special symmetry in the Hamiltonian, one needs at least two control parameters to possibly obtain real energy-level crossings in the Hamiltonian spectrum.

B. Geometric phase

B.1 Imaginary exponent

Quantum evolution of a closed system is unitary and hence it conserves the normalization condition on the system state $|\psi(t)\rangle$ at any time t

$$\langle\psi(t)|\psi(t)\rangle = 1\,. \tag{B.1}$$

Simply by taking the time derivative of this formula we obtain

$$\begin{aligned} 0 = \frac{\mathrm{d}}{\mathrm{d}t}\langle\psi(t)|\psi(t)\rangle = \left\langle\psi(t)\middle|\frac{\overleftarrow{\partial}}{\partial t}\middle|\psi(t)\right\rangle + \left\langle\psi(t)\middle|\frac{\overrightarrow{\partial}}{\partial t}\middle|\psi(t)\right\rangle = \\ = \left\langle\psi(t)\middle|\frac{\overrightarrow{\partial}}{\partial t}\middle|\psi(t)\right\rangle^* + \left\langle\psi(t)\middle|\frac{\overrightarrow{\partial}}{\partial t}\middle|\psi(t)\right\rangle = 2\,\mathrm{Re}\left\langle\psi(t)\middle|\frac{\partial}{\partial t}\middle|\psi(t)\right\rangle\,. \end{aligned} \tag{B.2}$$

It is therefore a general result that the quantity $\left\langle\psi(t)\middle|\frac{\partial}{\partial t}\middle|\psi(t)\right\rangle$ is purely imaginary.

The adiabatic evolution (2.5) reads

$$|\psi_n(t)\rangle = \exp\left(-i\int_0^t \mathrm{d}t' E_n(t')\right)\exp\left(-\int_0^t \mathrm{d}t'\left\langle n(t')\middle|\frac{\partial}{\partial t'}\middle|n(t')\right\rangle\right)|n(t)\rangle\,. \tag{B.3}$$

We see that the second term represents an additional phase factor called the *geometric phase*. To underline this fact, let us write

$$|\psi_n(t)\rangle = \exp\left(-i\int_0^t \mathrm{d}t' E_n(t')\right)\exp\Big(i\nu_n(t)\Big)|n(t)\rangle\,, \tag{B.4}$$

where we defined the geometric phase as

$$\nu_n(t) = i\int_0^t \mathrm{d}t'\left\langle n(t')\middle|\frac{\partial}{\partial t'}\middle|n(t')\right\rangle\,. \tag{B.5}$$

B.2 Time independence

Moreover, it is possible to show that the geometric phase does not depend on the evolution speed but only on the path taken in the configuration space (the space of parameters of the Hamiltonian).

Suppose a Hamiltonian $\hat{H}(\boldsymbol{R})$ with N parameters $R_1, \dots R_N$ and denote the instantaneous eigenstates $|n(\boldsymbol{R})\rangle$ corresponding to the exact values of parameters given by vector $\boldsymbol{R}$. External driving allows us to change the value of parameters $\boldsymbol{R}$ in time which introduces time-dependence also into the system Hamiltonian $\hat{H}(\boldsymbol{R}(t))$. Denote Γ the curve in the configuration space along which we drive the parameter vector $\boldsymbol{R}(t)$.

Let us reexpress the geometric phase ν_n in the language of externally driven Hamiltonian parameters by using the chain rule for $\frac{\partial}{\partial t'}$ and subsequent substitution rule,

$$\begin{aligned}\nu_n &= i\int_0^t \left\langle n(\boldsymbol{R}(t'))\middle|\frac{\partial}{\partial t'}\middle|n(\boldsymbol{R}(t'))\right\rangle \mathrm{d}t' = \\ &= i\int_0^t \sum_i \left\langle n(\boldsymbol{R}(t'))\middle|\frac{\partial}{\partial R_i}\middle|n(\boldsymbol{R}(t'))\right\rangle \frac{\mathrm{d}R_i}{\mathrm{d}t'}\,\mathrm{d}t' = \\ &= \int_\Gamma i\,\langle n(\boldsymbol{R})|\nabla_{\boldsymbol{R}}|n(\boldsymbol{R})\rangle\cdot\mathrm{d}\boldsymbol{R} = \nu_n(\Gamma)\,.\end{aligned} \tag{B.6}$$

The final formula clearly manifests time-independence as it is a path integral in the configuration space (thus depends only on Γ). This property is the reason behind the name geometric phase. The last integrand is called the *Berry connection*,

$$\boldsymbol{\mathcal{A}}_n(\boldsymbol{R}) = i\,\langle n(\boldsymbol{R})|\nabla_{\boldsymbol{R}}|n(\boldsymbol{R})\rangle\ . \tag{B.7}$$

C. More on Fidelity

The *fidelity* is a possible measure of closeness of two mixed quantum states [49]. It is a suitable quantity for quantum computing during which initially pure quantum states are turned into mixed ones. The reason for this phenomenon is the unavoidable presence of decoherence stemming from a trade-off between isolation from the environment and interaction strength among individual qubits. The properties of fidelity are therefore dealt with in quantum computing textbooks, such as [4].

The fidelity of two quantum states described by density matrices $\hat{\sigma}$ and $\hat{\rho}$ reads

$$\mathcal{F}(\hat{\sigma},\hat{\rho}) = \left[\mathrm{Tr}\,\sqrt{\sqrt{\hat{\sigma}}\,\hat{\rho}\sqrt{\hat{\sigma}}}\right]^2 \equiv \mathrm{Tr}^2\,\sqrt{\sqrt{\hat{\sigma}}\,\hat{\rho}\sqrt{\hat{\sigma}}}\,, \tag{C.1}$$

where we used symbol Tr^2 to simplify the notation. Note that the fidelity is sometimes in literature defined without the outer second power. Since density matrices are positive semi-definite, the square roots in (C.1) are defined as positive.

Thanks to the cyclic property of the trace, the fidelity is symmetric

$$\mathcal{F}(\hat{\sigma},\hat{\rho}) = \mathrm{Tr}^2\left[\sqrt[4]{\hat{\sigma}}\sqrt{\hat{\rho}}\sqrt[4]{\hat{\sigma}}\right] = \mathrm{Tr}^2\left[\sqrt{\hat{\sigma}}\sqrt{\hat{\rho}}\right] = \mathrm{Tr}^2\left[\sqrt{\hat{\rho}}\sqrt{\hat{\sigma}}\right] = \mathcal{F}(\hat{\rho},\hat{\sigma})\,. \tag{C.2}$$

As a consequence of Uhlmann's theorem [49, 4] it holds $\mathcal{F}(\hat{\sigma},\hat{\rho}) \in [0,1]$. By making use of the fact that the trace of a general density matrix is equal to 1, we obtain that the upper limit for fidelity is reached if the two states are equal, $\mathcal{F}(\hat{\rho},\hat{\rho}) = 1$.

Let us have a time-dependent Hamiltonian whose instantaneous eigenstates at time t are denoted $|k(t)\rangle$ and let $\hat{U}(t)$ be the evolution operator induced by this Hamiltonian from time 0 to time t. Suppose now, that $\hat{\sigma}$ corresponds to a pure quantum state $|k(t)\rangle$ and $\hat{\rho}$ is a mixed quantum state whose density matrix is diagonal in basis $\hat{U}(t)\,|k(0)\rangle$,

$$\hat{\sigma} = |k(t)\rangle\langle k(t)|\,, \tag{C.3}$$

$$\hat{\rho} = \sum_n p_n\,\hat{U}(t)\,|n(0)\rangle\langle n(0)|\,\hat{U}^\dagger(t)\,. \tag{C.4}$$

The fidelity of these two states read

$$\begin{aligned}\mathcal{F}_k(t) \equiv \mathcal{F}(\hat{\sigma},\hat{\rho}) = \mathrm{Tr}^2\,\sqrt{\hat{\sigma}\hat{\rho}\hat{\sigma}} = \mathrm{Tr}^2\,\sqrt{|k(t)\rangle\,\langle k(t)|\hat{\rho}|k(t)\rangle\,\langle k(t)|} = \\ = \mathrm{Tr}^2\left[|k(t)\rangle\langle k(t)|\,\sqrt{\langle k(t)|\hat{\rho}|k(t)\rangle}\right] = \langle k(t)|\hat{\rho}|k(t)\rangle\,,\end{aligned} \tag{C.5}$$

where we twice made use of the fact that a square root of a diagonal matrix corresponds to a square root of the individual diagonal elements. The last result holds for a general density matrix $\hat{\rho}$ and a pure state $|k(t)\rangle$. Let us now substitute for our particular case of $\hat{\rho}$,

$$\mathcal{F}_k(t) = \sum_n p_n \left|\left\langle k(t)\middle|\hat{U}(t)\middle|n(0)\right\rangle\right|^2. \tag{C.6}$$

The first case of interest is $p_n = \delta_{n0}$, corresponding to the evolution of the ground state. The second case of interest is the evolution of the thermal state,

for which

$$p_n = \frac{1}{Z(T)} \exp\left(-\frac{E_n(0)}{kT}\right) , \tag{C.7}$$

where T is the temperature, $Z(T)$ the corresponding partition function, k the Boltzmann constant and $E_n(0)$ is the instantaneous energy corresponding to state $|n(0)\rangle$.

Bibliography

[1] C. Gardinier and P. Zoller: *The Quantum World of Ultra-Cold Atoms and Light I: Foundations Of Quantum Optics*. Imperial College Press, 2014.

[2] C. Gardinier and P. Zoller: *The Quantum World of Ultra-Cold Atoms and Light II: The Physics of Quantum-Optical Devices*. Imperial College Press, 2015.

[3] C. Gardinier and P. Zoller: *The Quantum World of Ultra-Cold Atoms and Light III: Ultra-cold Atoms*. World Scientific Europe, 2017.

[4] M. A. Nielsen and I. L. Chuang: *Quantum Computation and Quantum Information*. Cambridge University Press, 2000.

[5] *The Independent: Quantum Computing*. URL: `http://www.independent.co.uk/topic/quantum-computing`.

[6] *Science Daily: Quantum Computers*. URL: `http://www.sciencedaily.com/news/computers_math/quantum_computers`.

[7] *Wired: Quantum Computing*. URL: `http://www.wired.com/tag/quantum-computing`.

[8] E. Farhi et al.: *Quantum Computation by Adiabatic Evolution* (2000). arXiv: quant-ph/0001106.

[9] T. Albash and D. A. Lidar, *Reviews of Modern Physics* **90**, 015002 (2018).

[10] A. D. King et al., *Nature* **560**, 456 (2018).

[11] S. Jiang et al., *Scientific Reports* **8**, 17667 (2018).

[12] J. Sanders: *D-Wave announces 5000-qubit fifth generation quantum annealer* (2019). URL: `http://www.techrepublic.com/article/d-wave-announces-5000-qubit-fifth-generation-quantum-annealer/` (visited on 7/16/2020).

[13] M. Born and V. Fock, *Zeitschrift für Physik* **51**, 165 (1928).

[14] T. Kato, *Journal of the Physical Society of Japan* **5**, 435 (1950).

[15] L. Landau, *Physikalische Zeitschrift der Sowjetunion* **2**, 46 (1932).

[16] C. Zener, *Proceedings of the Royal Society of London, Series A* **137**, 696 (1932).

[17] C. Wittig, *Journal of Physical Chemistry B* **109**, 8428 (2005).

[18] S. Sachdev: *Quantum Phase Transitions*. Cambridge University Press, 1999.

[19] L. D. Carr, editor: *Understanding Quantum Phase Transitions*. Taylor & Francis, 2010.

[20] H. J. Lipkin, N. Meshkov and A. J. Glick, *Nuclear Physics* **62**, 188 (1965); N. Meshkov, A. J. Glick and H. J. Lipkin, *Nuclear Physics* **62**, 199 (1965); A. J. Glick, H. J. Lipkin and N. Meshkov, *Nuclear Physics* **62**, 211 (1965).

[21] M. V. Berry, *Journal of Physics A: Mathematical and Theoretical* **42**, 365303 (2009).

[22] M. Demirplak and S. A. Rice, *Journal of Physical Chemistry A* **107**, 9937 (2003); M. Demirplak and S. A. Rice, *Journal of Physical Chemistry B* **109**, 6838 (2005).

[23] M. G. Bason et al., *Nature Physics* **8**, 147 (2011).

[24] A. del Campo, M. M. Rams and W. H. Zurek, *Physical Review Letters* **109**, 115703 (2012).

[25] P. Cejnar et al., *Journal of Physics A: Mathematical and General* **39**, L515 (2006).

[26] M. Caprio, P. Cejnar and F. Iachello, *Annals of Physics* **323**, 1106 (2008).

[27] D. Larese, F. Pérez-Bernal and F. Iachello, *Journal of Molecular Structure* **1051**, 310 (2013).

[28] T. Brandes, *Physical Review E* **88**, 032133 (2013).

[29] P. Stránský, M. Macek and P. Cejnar, *Annals of Physics* **345**, 73 (2014).

[30] M. A. Bastarrachea-Magnani, S. Lerma-Hernández and J. G. Hirsch, *Physical Review A* **89**, 032101 (2014).

[31] P. Stránský et al., *Annals of Physics* **356**, 57 (2015).

[32] P. Stránský and P. Cejnar, *Physics Letters A* **380**, 2637 (2016).

[33] M. Macek et al., *Physical Review C* **99**, 064323 (2019).

[34] F. Leyvraz and W. D. Heiss, *Physical Review Letters* **95**, 050402 (2005).

[35] P. Ribeiro, J. Vidal and R. Mosseri, *Physical Review Letters* **99**, 050402 (2007).

[36] P. Pérez-Fernández et al., *Physical Review A* **80**, 032111 (2009).

[37] L. F. Santos, M. Távora and F. Pérez-Bernal, *Physical Review A* **94**, 012113 (2016).

[38] M. Šindelka, L. F. Santos and N. Moiseyev, *Physical Review A* **95**, 010103 (2017).

[39] W. Kopylov et al., *New Journal of Physics* **17**, 013040 (2015).

[40] W. Kopylov and T. Brandes, *New Journal of Physics* **17**, 103031 (2015).

[41] I. M. Georgescu, S. Ashhab and F. Nori, *Reviews of Modern Physics* **86**, 153 (2014).

[42] J. Simon et al., *Nature* **472**, 307 (2011).

[43] R. Islam et al., *Nature Communications* **2**, 377 (2011).

[44] J. W. Britton et al., *Nature* **484**, 489 (2012).

[45] C. J. Foot: *Atomic Physics*. Oxford University Press, 2005.

[46] F. Haake: *Quantum Signatures of Chaos*. Springer, 2018.

[47] J. von Neumann, *Nachrichten von der Gesellschaft der Wissenschaften zu Göttingen, Mathematisch-Physikalische Klasse*, 273 (1927).

[48] L. E. Reichl: *A Modern Course in Statistical Physics*. Wiley-VCH, 2016.

[49] R. Jozsa, *Journal of Modern Optics* **41**, 2315 (1994).

[50] D. I. Tsomokos, S. Ashhab and F. Nori, *New Journal of Physics* **10**, 113020 (2008).

[51] Y. Zhou et al., *Physical Review A* **96**, 062333 (2017).

[52] J. Dolejší, Bachelor's thesis. Charles University, Faculty of Mathematics and Physics, Institute of Particle and Nuclear Physics. 2018.

[53] P. Cejnar and P. Stránský, *Physica Scripta* **91**, 083006 (2016).

[54] T. Holstein and H. Primakoff, *Physical Review* **58**, 1098 (1940).

[55] L. Fortnow, *Communications of the ACM* **52**, 78 (2009).

[56] O. Goldreich: *P, NP, and NP-Completeness: The Basics of Computational Complexity*. Cambridge University Press, 2010.

[57] M. Kloc, Master's thesis. Charles University, Faculty of Mathematics and Physics, Institute of Particle and Nuclear Physics. 2013.